SHAPE MATTERS:
A BROWNIAN MICROSWIMMER IN A CHANNEL

HONGFEI CHEN AND JEAN-LUC THIFFEAULT

Department of Mathematics, University of Wisconsin – Madison
480 Lincoln Dr., Madison, WI 53706, USA

ABSTRACT. We consider the active Brownian particle (ABP) model for a two-dimensional microswimmer with fixed speed, whose direction of swimming changes according to a Brownian process. The probability density for the swimmer evolves according to a Fokker–Planck equation defined on the configuration space, whose structure depends on the swimmer's shape, center of rotation and domain of swimming. We enforce zero probability flux at the boundaries of configuration space. We derive a reduced equation for a swimmer in an infinite channel, in the limit of small rotational diffusivity, and find that the invariant density depends strongly on the swimmer's precise shape and center of rotation. We also give a formula for the *mean reversal time*: the expected time taken for a swimmer to completely reverse direction in the channel. Using homogenization theory, we find an expression for the effective longitudinal diffusivity of a swimmer in the channel, and show that it is bounded by the mean reversal time.

[*Note to reader: we have included a table of notation in Appendix B.*]

1. INTRODUCTION

Microswimmers are common in nature — they include bacteria, spermatozoa, some algae, and synthetic swimmers. In almost all contexts these swimmers interact with boundaries, either biological (e.g., the gut, cell walls) or man-made (e.g., tubes, filters). These interactions have been studied experimentally, numerically, and theoretically by many groups. The two main aspects of interaction are hydrodynamic (mediated by the fluid) and steric (direct contact with the boundary); they can have different relative importance depending on the context, but it is widely accepted that both can play a crucial role [7, 14, 21, 39].

In the present paper we will be concerned with modeling the steric interaction of a microswimmer with solid surfaces, with an emphasis on the role of the swimmer's

---

shape. For simplicity, the swimmer will be two dimensional with a fixed shape, though in principle the theory could be extended to include a deformable body or flagella.

1.1. **Previous work.** Many models have been proposed to mimic the behavior of microswimmers, with the simplest being the *active Brownian particle* (ABP) model [1, 81, 98, 102, 116, 125] where a particle moves with constant speed and both its swimming direction and spatial position are subject to independent diffusion processes. A more complicated model has the organism moving in a straight line for a random time (run), followed by a random change in direction (tumble); such run-and-tumble models have been investigated both theoretically and numerically [10, 11, 15, 24, 25, 27, 28, 45, 50, 54, 61, 62, 66, 70, 74, 75, 80, 94, 104]. There are also more complex models that incorporate hydrodynamic effects [3, 8, 15–18, 26, 30, 59, 63, 65, 66, 71, 78, 84, 86–90, 92, 96, 100, 106–110, 115, 119, 123]. In the present paper we will limit ourselves to the ABP model.

Experiments with microswimmers near boundaries are also plentiful [6, 14, 20, 21, 31, 36, 39, 44, 51, 57, 83, 113, 120]. As early as 1963, Rothschild [83] measured the density of bull spermatozoa between two glass plates and found accumulation near the plates. Accumulation as well as local alignment and preferred tail rotation were also observed in later experiments [6, 14, 19, 21, 36, 39, 51, 55–57, 83, 113, 120]. Simulations have shown that either hydrodynamic interactions or steric interactions with thermal fluctuations can lead to accumulation. Later work found that steric effects dominate at walls, while hydrodynamic interactions can play an important role depending on the shape of the swimmer and its orientation with respect to the wall [7, 14, 21, 39].

In principle, the interaction of microswimmers with boundaries requires modeling both hydrodynamic and steric interactions. Some groups include only hydrodynamic interactions [16, 17, 22, 34, 40–43, 60, 73, 78, 87, 93, 97, 99, 100, 103, 108, 115], which can be done in several ways: either explicitly with a solution of the Stokes equation, or implicitly through a resistance or mobility matrix, with various approximations in both cases. Spagnolie & Lauga [99] used a multipole expansion which in principle can be applied to any swimmer shape, and Takagi *et al.* [105] solved the Stokes equation in the lubrication limit. Zargar *et al.* [124] approximated the mobility matrix by restricting the swimmer to planar motion near a wall. Despite the simplifications in these models, they are fairly accurate away from boundaries and reproduce observed behavior [5, 52, 68, 125]. However, such models remain in general fairly complicated and either ignore the details of swimmers such as shape, or are swimmer-dependent. Most importantly, they ignore steric interactions and hence are not accurate near walls.

Steric interactions are often included phenomenologically, such as by using wall potential functions [9, 13, 15, 18, 35, 38, 71, 95, 111, 112, 115, 118]. This approach makes it easy to add boundaries to free-space simulations and has low simulation cost. Sepúlveda *et al.* [95] used Weeks–Chandler–Anderson functions and a Gaussian potential function for deformable swimmers; they treat the effective wall force as a smooth repulsive force. Hernandez-Ortiz *et al.* [35] used Gay–Berne functions for steric exclusion of rod-shape swimmers. These models are usually a smooth approximation to the true dynamics, whereas for rigid swimmers the steric effect is by volume exclusion. Moreover, the complicated potential functions make it hard to obtain predictive formulas, although some authors used a simple harmonic potential to represent an elastic boundary, which made the problem tractable [9, 21, 76].

Another way to model steric interactions is to assign specific dynamics near the boundary such as reflecting [11, 45, 58, 114] or vanishing velocity [95] boundary conditions. It is worth noting that neither boundary condition is realistic. Ezhilan *et al.* [29] observed that reflecting boundary conditions do not recover the behavior observed in experiments. Other groups did not try to prescribe any specific law for swimmers at a boundary and focused on statistics such as the invariant density of swimmers [28, 121, 122] and swim pressure [9, 11, 101, 121].

When modeling a collection of stochastic swimmers or the statistics of a single swimmer, an ideal approach to include steric interactions is to use no-flux boundary conditions that prevent the organism's body from entering the wall, as described by Nitsche & Brenner [77] for passive particles. Most work in the literature using these boundary conditions assumes that swimmers have negligible size or are of spherical shape, so that they can rotate freely at a wall [2–4, 29, 121, 122]. Lee *et al.* [53] attempted to solve for the invariant density without spatial diffusion for point swimmers in a channel, and managed to find a solution when swimmers had only six swimming directions. Wagner *et al.* [116] continued Lee's work and found the invariant density for continuous swimming directions by introducing a wall density function. Schaar *et al.* [93] later calculated the trapping time at a wall. Ai *et al.* [1] predicted for point swimmers the optimal swimming speed, the spatial diffusion, and the strength of wall potentials for maximal effective diffusion. For spherical or point swimmers, Elgeti & Gompper [23] and Ezhilan & Saintillan [29] investigated asymptotic solutions to the Fokker–Planck equation associated with the ABP model. Elgeti & Gompper [25] subsequently found the invariant density for run-and-tumble spherical swimmers.

1.2. **The role of shape.** The admissible positions and orientations of a nonspherical swimmer are constrained by the presence of walls; the set of admissible values of the degrees of freedom is the *configuration space* [77] (see Section 2). A natural way to include the shape of a swimmer into a model is thus to impose no-flux boundary
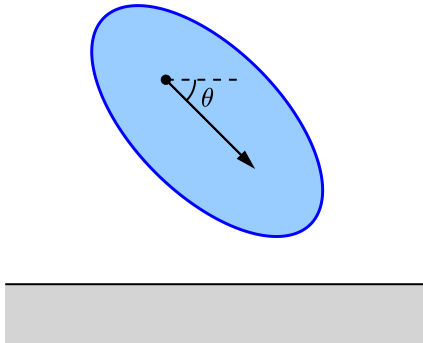
FIGURE 1. An elliptical swimmer approaching a wall at a direction $\theta = -\pi/4$. The center of rotation is not necessarily the geometric center of the ellipse.

conditions on the configuration space itself. Krochak *et al.* [46] and Ezhilan *et al.* [29] used steric exclusion with no-flux boundary conditions for rigid fibers and rod-like swimmers, respectively, and simulated the invariant density in a channel in the presence of flow.

In the present paper we propose a framework to incorporate the shape of a swimmer into the boundary conditions of a partial differential equation describing its dynamics. The PDE is the Fokker–Planck equation derived from the two-dimensional ABP model with no-flux boundary conditions in configuration space. The configuration space is determined by the swimmer's shape and the domain of swimming, which we take to be an infinite channel. We solve explicitly for the invariant density in the limit of small rotational diffusivity. In the same limit, we also solve for the mean reversal time and the longitudinal effective diffusivity of the swimmer. All these quantities are greatly influenced by the shape of the swimmer. In particular the effective diffusivity can become very large when the swimmer tends to align parallel to the channel walls, which can surprisingly occur even for circular swimmers when their center of rotation does not coincide with the geometric center (see below).

An important observation is in order regarding the ABP model for a finite-size swimmer. The ABP model implicitly assumes that the swimmer rotates about some distinguished fixed point in a co-moving frame. The precise location of this point becomes important when the swimmer has finite size and boundaries are present. For example, Figure 1 shows an elliptical swimmer approaching a boundary: the direction of swimming is given by the angle θ, which is measured counterclockwise from the horizontal, so that $\theta < 0$ corresponds to swimming towards the wall. The angle θ is measured around a point we call the *center of rotation* of the swimmer. For a free particle, this corresponds to the *center of hydrodynamic reaction* defined

by Happel & Brenner [33, p. 174]. For an ellipse it would coincides with the geometrical center. However, the swimmer's propulsion mechanism (e.g., flagella), which is abstracted here since we consider fixed shapes, can displace this center. Hence, we treat the center of rotation as a parameter that may be adjusted to model a particular swimmer. To parallel terminology based on the type of propulsion used by a microorganism [34, 35, 89, 91], when the center of rotation is ahead of the geometric center we will call the swimmer *puller-like*; when it is behind we call it *pusher-like*. If the swimmer doesn't interact with boundaries, then the center of rotation is not particularly important to the dynamics; but with external boundaries it can influence the tendency of the swimmer to align parallel or perpendicular to a wall, depending on its shape [64]. In fact, we will see that even a circular particle can align with a wall if its center of rotation is behind the geometric center, despite the absence of hydrodynamic interactions.

1.3. **Outline.** In this paper we focus exclusively on a two-dimensional swimmer undergoing steric interactions. In Section 2 we describe the configuration space for a swimmer with an arbitrary fixed convex shape, in particular when the swimmer is confined to a channel consisting of two infinite parallel walls. A crucial quantity is the *wall distance function*, which describes the swimmer's closest point of approach to a wall as a function of the swimmer's orientation. We give explicit examples for needle (rod-like), elliptical, and teardrop-shaped swimmers. The wall distance function can then be used twice to determine the full configuration space in a channel. This configuration space is *open* if the swimmer can reverse direction in the channel, or *closed* if the channel is too narrow to do so. We also describe symmetries of the configuration space that follow from symmetries of the swimmer and channel, the most important being the case where a swimmer is *left-right symmetric*.

In Section 3 we describe the stochastic ABP model for our swimmer, and give its corresponding Fokker–Planck equation. This leads to the natural no-flux boundary conditions that we impose at the solid walls. For the infinite channel geometry we average over the lengthwise coordinate. In Section 4 we simplify the model by assuming a small rotational diffusivity. This leads to a *reduced equation*, which is a partial differential equation in one time variable and one angle. The configuration geometry is completely encoded into a single effective angular drift function.

In Section 5 we solve for the steady state of the reduced equation, which gives us the *invariant probability density* of the swimmer, or invariant density for short. The invariant density is strongly dependent on the shape and center of rotation, as we show with some explicit examples, typically in the limit of rapid swimming. In particular, we show that circular swimmers can align either parallel or perpendicular to the walls, depending on whether they are pusher- or puller-like, respectively.

When a swimmer has broken left-right symmetry, it can undergo a net rotation due to repeated biased interactions with the walls.

We introduce the *mean reversal time* (MRT) of a swimmer in Section 6: the expected time for a swimmer to fully reverse direction in an open channel. This is a generalization of the turnaround time of Holcman & Schuss [37], who described the expected time for a Brownian needle to reverse direction when its length is slightly shorter than the channel width. For a left-right symmetric swimmer we give a simple integral formula for the MRT. We explicitly compute the MRT in some limits, in particular for a fast swimmer. The MRT in this fast case is exponentially long, since the swimmer sticks to a wall for a very long time before undergoing a large enough random fluctuation that causes reversal.

In Section 7 we use a homogenization theory approach to find the longitudinal *effective diffusivity* D_{eff} for the swimmer in an open channel. In the same reduced limit as above (small rotational diffusion) we give an integral formula for the diffusivity. For a fast swimmer we might expect that the effective diffusivity is related to the MRT: the swimmer makes large excursions and sometimes reverses direction, thereby undergoing an effective random walk for long times. Indeed, we obtain the rigorous bound

$$D_{\mathrm{eff}} \leq D_X + \tfrac{1}{2}\tau_{\mathrm{rev}}\, U^2,$$

where D_X is the diffusivity of the swimmer along the direction of swimming, τ_{rev} is the MRT, and U is the swimming speed. The term $\frac{1}{2}(\tau_{\mathrm{rev}}\, U)^2/\tau_{\mathrm{rev}}$ is equal to the diffusivity for an unbiased random walk with step size $\tau_{\mathrm{rev}}U$ and step time τ_{rev}. Finally, we offer some concluding remarks in Section 8.

2. CONFIGURATION SPACE

In this section we describe how the swimmer's shape interacts with boundaries to create *configuration space*. We first establish coordinate systems for a convex swimmer (Section 2.1): the fixed lab frame and a frame rotating with the swimmer. These are both necessary since the direction of swimming and the magnitude of diffusion are tied to the swimmer's shape, and may be different along different axes (Section 3). We use the term "swimmer" throughout, but our entire formalism applies to passive particles as well, for which $U = 0$. We consider an arbitrary contact point between a swimmer's body and a single wall, and show how to derive the *wall distance function* for the swimmer. We present a few examples: a needle (one-dimensional segment), an ellipse, and a 'teardrop' shape. These are all swimmers with a left-right axis of symmetry, but our formalism applies to more general swimmers as well.

In Section 2.2 we use the wall distance function to obtain the configuration space for a swimmer confined between two infinite, parallel walls. Two very different cases emerges: in the *open* channel configuration the channel is wide enough to allow the
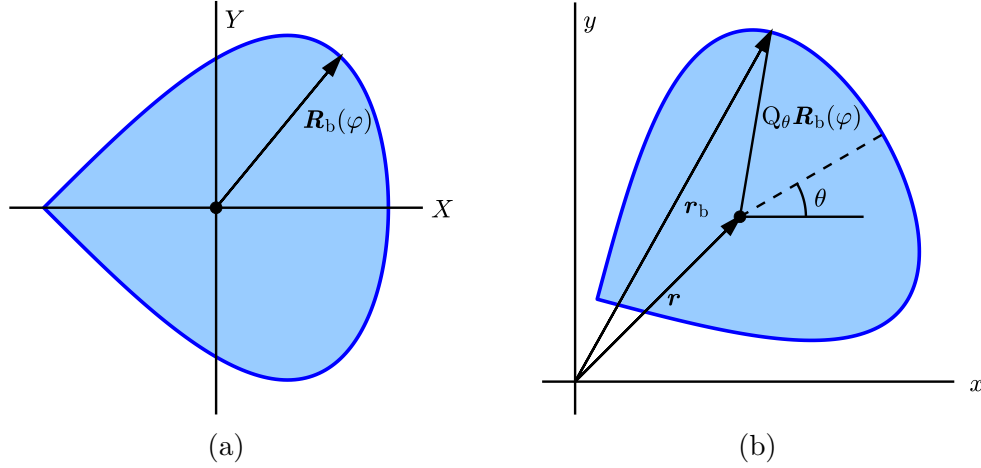
FIGURE 2. Boundary of a convex swimmer in (a) the swimmer's frame, with the swimming direction along the positive X axis, and (b) the fixed lab frame, where the swimming direction makes an angle θ with the x axis.

swimmer to completely reverse direction, whereas in the *closed* configuration the swimmer is unable to do so.

2.1. **The wall distance function.** The shape of a swimmer is expressed by giving its boundary in parametric form

$$\boldsymbol{R} = \boldsymbol{R}_{\mathrm{b}}(\varphi) = (X_{\mathrm{b}}(\varphi), Y_{\mathrm{b}}(\varphi)), \qquad -\pi < \varphi \leq \pi, \tag{2.1}$$

where $\boldsymbol{R}_{\mathrm{b}}(\varphi)$ is a 2π-periodic, piecewise-smooth function (Fig. 2a). By convention, the swimming direction $\boldsymbol{R}_{\mathrm{b}}(0)$ is along the positive X axis in the swimmer's co-moving and co-rotating frame. The origin of the $\boldsymbol{R} = (X, Y)$ coordinate system is the *center of rotation* of the swimmer. Note that we do not require $\tan \varphi = Y_{\mathrm{b}}(\varphi)/X_{\mathrm{b}}(\varphi)$, that is, φ does not necessarily correspond to the polar angle of $\boldsymbol{R}_{\mathrm{b}}(\varphi)$.

In a fixed (lab) frame, the boundary of the swimmer is located at (Fig. 2b)

$$(x_{\mathrm{b}}, y_{\mathrm{b}}) = \boldsymbol{r}_{\mathrm{b}}(\theta, \varphi) = \boldsymbol{r} + \mathbb{Q}_\theta \cdot \boldsymbol{R}_{\mathrm{b}}(\varphi), \qquad -\pi < \varphi, \theta \leq \pi, \tag{2.2}$$

where $\boldsymbol{r} = (x, y)$ denotes the center of rotation of the swimmer and

$$\mathbb{Q}_\theta = \begin{pmatrix} \cos \theta & -\sin \theta \\ \sin \theta & \cos \theta \end{pmatrix} \tag{2.3}$$
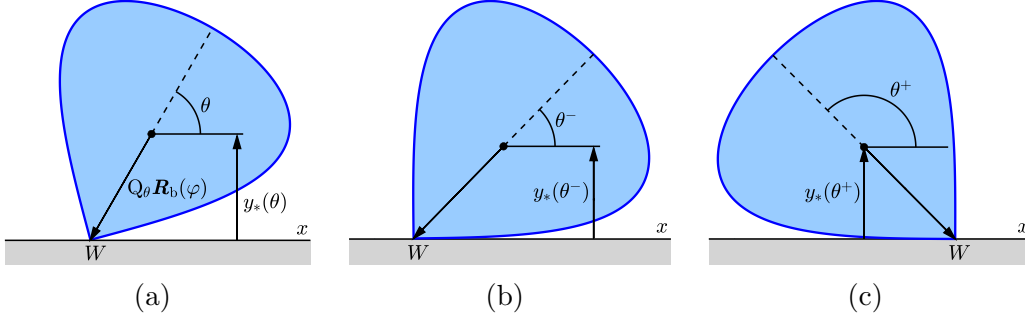
is a rotation matrix.

(a)   (b)   (c)

FIGURE 3. (a) Convex swimmer touching a horizontal wall at a corner point W. (b)–(c) Holding W fixed, the angle θ can vary from the right-tangency angle θ^- to the left-tangency angle θ^+.

Now take the swimmer to be touching an infinite wall along $y = 0$, as shown in Fig. 3a. The contact point W between the swimmer and the wall has coordinates

$$(x_\mathrm{b}, 0) = \boldsymbol{r} + \mathbb{Q}_\theta \cdot \boldsymbol{R}_\mathrm{b}(\varphi). \tag{2.4}$$

We wish to solve for the swimmer's center of rotation $\boldsymbol{r} = (x, y)$, which depends only on the convex hull of the swimmer; hence the swimmer's shape may be assumed convex without loss of generality. We proceed differently depending on whether the contact point W is a corner or a smooth boundary point. (Note that the analysis below can be couched in the language of Legendre transformations and convex analysis, but we opt here for a direct treatment.)

2.1.1. *Corner.* Consider first the case where the contact point W corresponds to a corner of the piecewise-smooth boundary, as in Fig. 3a. The parameter φ has a fixed value for corner W. The allowable range of θ is then determined by the right- and left-tangency values of θ:

$$\theta^- \leq \theta \leq \theta^+, \qquad \tan\theta^\pm = -Y_\mathrm{b}'(\varphi^\pm)/X_\mathrm{b}'(\varphi^\pm), \tag{2.5}$$

as depicted in Figs. 3b and 3c. For this range of θ, we can then use Eq. (2.4) to deduce the range of y values:

$$y_*(\theta) = -\sin\theta\, X_\mathrm{b}(\varphi) - \cos\theta\, Y_\mathrm{b}(\varphi), \qquad \theta^- \leq \theta \leq \theta^+. \tag{2.6}$$

We call y_* the *wall distance function*. It characterizes the minimum distance from the swimmer's center of rotation to a wall at $y_\mathrm{b} = 0$, as a function of the swimmer's orientation. Observe that a given corner corresponds to a single φ value, but a range of θ values.

Example 1 (needle swimmer). As a simple example, take

$$X_{\mathrm{b}}(\varphi) = \tfrac{1}{2}\ell \cos\varphi - X_{\mathrm{rot}}, \qquad Y_{\mathrm{b}}(\varphi) = 0. \tag{2.7}$$

This is the *needle swimmer* with center of rotation at $X = X_{\mathrm{rot}}$, with $|X_{\mathrm{rot}}| \le \ell/2$. It consists of a one-dimensional segment of length ℓ, with degenerate "corners" at $\varphi_1 = 0$ and $\varphi_2 = \pi$. At $\varphi = \varphi_1 = 0$, we have $-\pi \le \theta \le 0$, so from Eq. (2.6) $y_*(\theta) = -\sin\theta\, X_{\mathrm{b}}(\varphi_1) = -\sin\theta(\tfrac{1}{2}\ell - X_{\mathrm{rot}})$. At $\varphi = \varphi_2 = \pi$, we have $0 \le \theta \le \pi$, so from Eq. (2.6) $y_*(\theta) = -\sin\theta\, X_{\mathrm{b}}(\varphi_2) = -\sin\theta(-\tfrac{1}{2}\ell - X_{\mathrm{rot}})$. We can combine these cases by writing

$$y_*(\theta) = \tfrac{1}{2}\ell|\sin\theta| + X_{\mathrm{rot}}\sin\theta, \qquad -\pi < \theta \le \pi. \tag{2.8}$$

Only needle positions with $y \ge y_*(\theta)$ are allowed; see Figs. 4a and 4b for a plot. For the case $X_{\mathrm{rot}} = 0$, this type of swimmer and configuration space was investigated by Ezhilan & Saintillan [29]. △

We will typically use ℓ to denote the maximum diameter of a swimmer, which controls whether or not it can reverse direction for a given channel width (Section 2.2). The parameter X_{rot} controls the position of the center of rotation: for $X_{\mathrm{rot}} > 0$ it is closer to the front, and for $X_{\mathrm{rot}} < 0$ it is towards the rear. We often refer to these cases as *puller-like* and *pusher-like*, respectively, by analogy with the classification based on the type of propulsion used by a microorganism [34, 35, 89, 91].

2.1.2. *Smooth boundary point.* When the contact point W is at a smooth boundary point, given θ we wish to solve for (x, y) and φ. Two equations come from (2.4), but we need a third, which stems from requiring that the tangent to the swimmer,

$$\boldsymbol{t}_{\mathrm{b}} = \partial_\varphi \boldsymbol{r}_{\mathrm{b}} = \mathbb{Q}_\theta \cdot \boldsymbol{R}'_{\mathrm{b}}(\varphi), \tag{2.9}$$

is horizontal at W:

$$X'_{\mathrm{b}}(\varphi)\sin\theta + Y'_{\mathrm{b}}(\varphi)\cos\theta = 0 \tag{2.10}$$

or

$$Y'_{\mathrm{b}}(\varphi)/X'_{\mathrm{b}}(\varphi) = -\tan\theta. \tag{2.11}$$

We can solve Eq. (2.11) for $\varphi = \varphi_*(\theta)$, which we then use in Eq. (2.4) to obtain $\boldsymbol{r} = \boldsymbol{r}_*(\theta)$ at the contact point:

$$\boldsymbol{r}_*(\theta) = (x_*(\theta), y_*(\theta)) = -\mathbb{Q}_\theta \cdot \boldsymbol{R}_{\mathrm{b}}(\varphi_*(\theta)). \tag{2.12}$$

Equation (2.11) can have more than one solution, but we keep the one that leads to a non-negative wall distance function,

$$y_*(\theta) = -\sin\theta\, X_{\mathrm{b}}(\varphi_*(\theta)) - \cos\theta\, Y_{\mathrm{b}}(\varphi_*(\theta)) \ge 0. \tag{2.13}$$

(a)

(b)

(c)

(d)

(e)

(f)

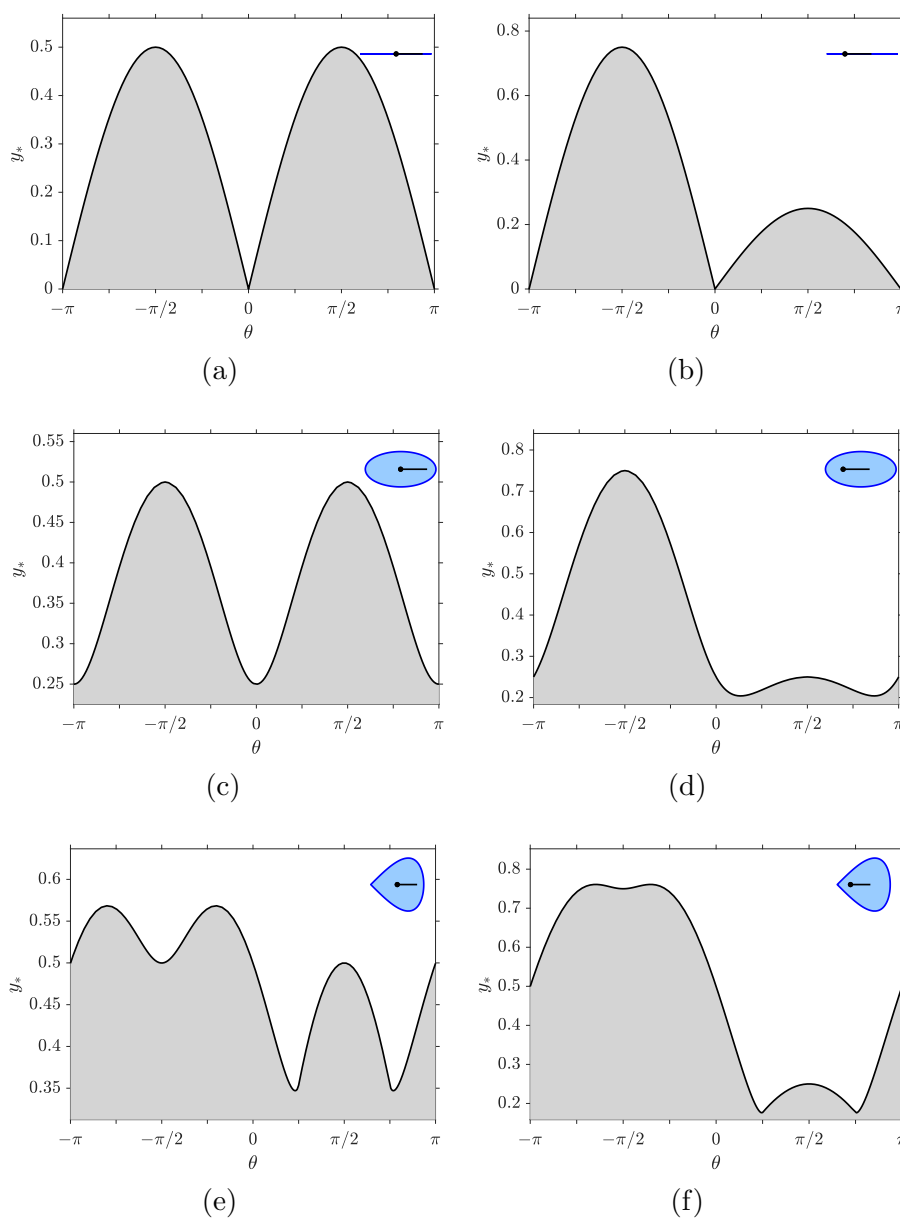FIGURE 4. The wall distance function $y_*(\theta)$ for three different swimmers: (a,b) needle of length $\ell = 2a = 1$; (c,d) ellipse of length $\ell = 2a = 1$ and width $2b = 1/2$; (e,f) teardrop-shaped swimmer of size 1 by 1. The inset shows the swimmer shape and center of rotation, with swimming direction to the right. The right column has center of rotation displaced to $X_{\mathrm{rot}} = -1/4$.

Example 2 (elliptical swimmer). An ellipse-shaped swimmer with semi-axes a and b can be parameterized as

$$X_{\mathrm{b}}(\varphi) = a\cos\varphi - X_{\mathrm{rot}}, \qquad Y_{\mathrm{b}}(\varphi) = b\sin\varphi \tag{2.14}$$

with $|X_{\mathrm{rot}}| \leq a$. Here a and b are the semi-axes along and perpendicular to the swimming direction, respectively. The tangency condition (2.11) is then $\cot\varphi_*(\theta) = (a/b)\tan\theta$. After inserting in Eq. (2.13) and selecting the non-negative solution we obtain

$$y_*(\theta) = \sqrt{a^2\sin^2\theta + b^2\cos^2\theta} + X_{\mathrm{rot}}\,\sin\theta. \tag{2.15}$$

This wall distance function is plotted in Figs. 4c and 4d.

For $a \geq b$, it is convenient to rewrite (2.15) as

$$y_*(\theta) = a\sqrt{1 - e^2\cos^2\theta} + X_{\mathrm{rot}}\,\sin\theta, \qquad e := \sqrt{1 - b^2/a^2} < 1, \tag{2.16}$$

where e is the eccentricity. For $b = 0$ ($e = 1$) we recover the needle case Eq. (2.8), with $a = \ell/2$. The case $e = 0$ is a circular swimmer, which for $X_{\mathrm{rot}} = 0$ has the same dynamics in our model as a point swimmer [23, 53]. Note however that for $X_{\mathrm{rot}} \neq 0$ even a circular swimmer can exhibit alignment with the walls (see Example 6). $\triangle$

2.1.3. *General shapes.* The convex hull for a general swimmer will consist of a combination of smooth parts separated by corners, as for the 'teardrop' swimmer depicted in Fig. 2. The wall distance function $y_*(\theta)$ cannot be found analytically in general, but is easy to compute numerically. The simplest approach is to discretize the convex hull as a polygon, and then apply the formulas in Section 2.1.1 to every corner.

Example 3 (teardrop swimmer). The 'teardrop' swimmer depicted in Fig. 2 is parameterized by

$$X_{\mathrm{b}}(\varphi) = a(2|\cos(\varphi/2)| - 1) - X_{\mathrm{rot}}, \qquad Y_{\mathrm{b}}(\varphi) = b\sin\varphi \tag{2.17}$$

with $|X_{\mathrm{rot}}| \leq a$. This shape has a smooth boundary except for one corner at $\varphi = \varphi_1 = \pi$. The wall distance function can be obtained analytically but is a bit cumbersome; we plot it in Figs. 4e and 4f. Unlike the previous examples, the wall distance function for the teardrop swimmer has a local *minimum* at $\theta = -\pi/2$, rather than a maximum. This value of θ corresponds to swimming towards the wall, and the minimum suggests that this shape has a tendency to align perpendicular to the wall, rather than parallel. (This is similar to the triangular swimmer in Lushi *et al.* [64].) In the presence of diffusion, the depth of the local minimum is a measure of how long a swimmer gets stuck in that position before fluctuating out. See also Example 6 for another, simpler model swimmer that aligns perpendicular to the wall. $\triangle$

All the examples discussed thus far involve *left-right symmetric swimmers*, which satisfy $(X_{\mathrm{b}}(\varphi), Y_{\mathrm{b}}(\varphi)) = (X_{\mathrm{b}}(-\varphi), -Y_{\mathrm{b}}(-\varphi))$. For this class of swimmers, the wall

distance function has the symmetry

$$y_*(\theta) = y_*(\pi - \theta) \tag{2.18}$$

which is evident in Fig. 4.

2.2. **Channel geometry.** So far we have considered a two-dimensional swimmer above a single infinite horizontal wall. In a channel geometry, the swimmer is confined between two parallel infinite walls, at $y = \pm L/2$. Luckily, we do not need to derive a separate wall distance function for the top wall: we can deduce it by symmetry. The center of rotation of a swimmer with wall distance function $y_*(\theta)$ will have its y coordinate in the range

$$\zeta_-(\theta) \le y \le \zeta_+(\theta) \tag{2.19}$$

where

$$\zeta_-(\theta) = y_*(\theta) - L/2, \qquad \zeta_+(\theta) = -y_*(\theta + \pi) + L/2. \tag{2.20}$$

This means that $\zeta_\pm$ are related by the *channel symmetry*

$$\zeta_+(\theta) = -\zeta_-(\theta + \pi). \tag{2.21}$$

The x coordinate of the center of rotation is unconstrained and can be any real number, but the domain for the swimming angle θ can either be $[-\pi, \pi]$ or a union of disjoint intervals. This depends on whether $\zeta_-(\theta) < \zeta_+(\theta)$ for all $\theta \in [-\pi, \pi]$, or $\zeta_+(\theta) = \zeta_-(\theta)$ for some θ. We call these two cases the *open channel* and the *closed channel*, respectively.

2.2.1. *Open channel.* In the simplest case, we have

$$\theta \in [-\pi, \pi], \qquad \zeta_-(\theta) < \zeta_+(\theta). \tag{2.22}$$

In this case the swimmer can fully reverse direction in the channel. The full configuration space for the swimmer's center of rotation is then

$$\Omega = \{(x, y, \theta) : x \in \mathbb{R}, \ \zeta_-(\theta) \le y \le \zeta_+(\theta), \ -\pi \le \theta \le \pi\} \tag{2.23}$$

periodic in the θ direction. This configuration space is depicted in Fig. 5a.

2.2.2. *Closed channel.* Another possibility is that $\zeta_+(\theta_i) = \zeta_-(\theta_i)$ for some set of points $\{\theta_i\}$. This breaks up $[-\pi, \pi]$ into inadmissible intervals where $\zeta_-(\theta) > \zeta_+(\theta)$, and N disjoint admissible intervals

$$\theta \in (\theta_i^{\mathrm{L}}, \theta_i^{\mathrm{R}}), \quad \text{with} \quad \zeta_-(\theta) < \zeta_+(\theta), \qquad i = 1, \ldots, N. \tag{2.24}$$

The relevant interval is determined by the initial orientation of the swimmer. The motion of the swimmer then takes place in the configuration space

$$\Omega_i = \{(x, y, \theta) : x \in \mathbb{R}, \ \zeta_-(\theta) \le y \le \zeta_+(\theta), \ \theta_i^{\mathrm{L}} \le \theta \le \theta_i^{\mathrm{R}}\} \tag{2.25}$$
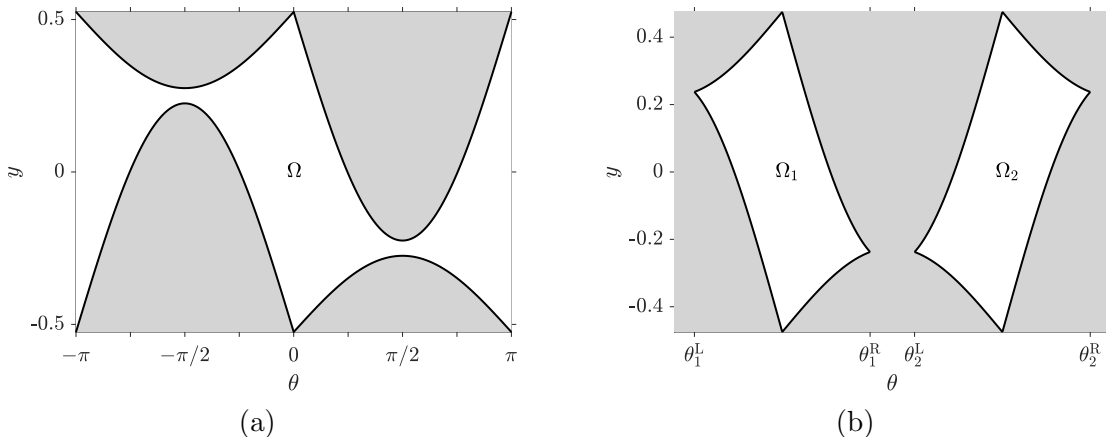
(a)   (b)

FIGURE 5. Configuration space for the needle in Fig. 4b of length $\ell = 2a = 1$ in (a) an open channel of width $L = 1.05$; (b) a closed channel of width $L = 0.95$. (x direction not shown.)

which is *not* periodic in the θ direction. This configuration space is depicted in Fig. 5b. Note that the condition $\zeta_+(\theta_i) = \zeta_-(\theta_i)$ together with the channel symmetry (2.21) implies that $\zeta_+(\theta_i + \pi) = \zeta_-(\theta_i + \pi)$.

3. STOCHASTIC MODEL

Now that we've established that the domain of motion for our swimmer is described by the configuration space of Section 2, we now describe the stochastic model for the swimmer's motion, the active Brownian particle model (ABP).

3.1. **Derivation from the SDE.** In the ABP model, the Brownian swimmer obeys the stochastic equation

$$\mathrm{d}X = U\mathrm{d}t + \sqrt{2D_X}\,\mathrm{d}W_1\,; \tag{3.1a}$$

$$\mathrm{d}Y = \sqrt{2D_Y}\,\mathrm{d}W_2\,; \tag{3.1b}$$

$$\mathrm{d}\theta = \sqrt{2D_\theta}\,\mathrm{d}W_3, \tag{3.1c}$$

in its own rotating reference frame. (We omitted any intrinsic swimmer rotation for simplicity, though this would not change the derivation appreciably. We will see that a net rotation can still emerge when the swimmer is not left-right symmetric.) In

terms of absolute x and y coordinates, this becomes an Itô stochastic equation

$$\mathrm{d}x = \left(U\mathrm{d}t + \sqrt{2D_X}\,\mathrm{d}W_1\right)\cos\theta - \sin\theta\,\sqrt{2D_Y}\,\mathrm{d}W_2\,; \tag{3.2a}$$

$$\mathrm{d}y = \left(U\mathrm{d}t + \sqrt{2D_X}\,\mathrm{d}W_1\right)\sin\theta + \cos\theta\,\sqrt{2D_Y}\,\mathrm{d}W_2\,; \tag{3.2b}$$

$$\mathrm{d}\theta = \sqrt{2D_\theta}\,\mathrm{d}W_3\,. \tag{3.2c}$$

For now we take U, D_X, D_Y, D_θ to be general functions of (x, y, θ, t). The corresponding Fokker–Planck equation for the probability density $p(x, y, \theta, t)$ is then

$$\partial_t p = -\nabla \cdot (\boldsymbol{U}p - \nabla \cdot (\mathbb{D}\,p)) + \partial_\theta^2(D_\theta\,p) \tag{3.3}$$

where $\nabla := \hat{\boldsymbol{x}}\,\partial_x + \hat{\boldsymbol{y}}\,\partial_y$, and the drift vector and diffusion tensor are respectively

$$\boldsymbol{U} = \begin{pmatrix} U\cos\theta \\ U\sin\theta \end{pmatrix}, \qquad \mathbb{D} = \begin{pmatrix} D_X\cos^2\theta + D_Y\sin^2\theta & \frac{1}{2}(D_X - D_Y)\sin 2\theta \\ \frac{1}{2}(D_X - D_Y)\sin 2\theta & D_X\sin^2\theta + D_Y\cos^2\theta \end{pmatrix}. \tag{3.4}$$

See Kurzthaler *et al.* [48, 49] for the intermediate scattering function for Eq. (3.3) in the absence of boundaries and with constant parameters.

For any fixed volume V we have

$$\partial_t \int_V p\,\mathrm{d}V = -\int_V \left(\nabla \cdot (\boldsymbol{U}p - \nabla \cdot (\mathbb{D}\,p)) - \partial_\theta^2(D_\theta\,p)\right)\mathrm{d}V$$

$$= -\int_{\partial V} \boldsymbol{f} \cdot \mathrm{d}\boldsymbol{S}\,, \tag{3.5}$$

where ∂V is the boundary of V, and the flux vector is

$$\boldsymbol{f} = \boldsymbol{U}p - \nabla \cdot (\mathbb{D}\,p) - \hat{\boldsymbol{\theta}}\,\partial_\theta(D_\theta\,p). \tag{3.6}$$

Thus, on the reflecting parts of the boundary we require the no-flux condition

$$\boldsymbol{f} \cdot \boldsymbol{n} = 0, \quad \text{on} \quad \partial V, \tag{3.7}$$

where $\boldsymbol{n}$ is normal to the boundary.

3.2. **Infinite channel geometry.** The previous section applies to any geometry and general $\boldsymbol{U}$, $\mathbb{D}$, and D_θ, which can be functions of (x, y, θ, t). For our problem, these only depend on θ. In an infinite channel geometry (Section 2.2), which we consider in this paper, we can eliminate the along-channel direction x by defining the marginal probability density

$$\bar{p}(y, \theta, t) = \int_{-\infty}^\infty p(x, y, \theta, t)\,\mathrm{d}x. \tag{3.8}$$

In order for $\bar{p}$ to be finite, p has to decay fast enough as $|x| \to \infty$; we use this assumption to discard some terms after we integrate Eq. (3.3) from $x = -\infty$ to ∞,

and find an equation for $\bar{p}$:

$$\partial_t \bar{p} = -\partial_y(U \sin\theta \, \bar{p}) + \partial_y^2(D_{yy} \, \bar{p}) + \partial_\theta^2(D_\theta \, \bar{p}) \tag{3.9}$$

where from (3.4) $D_{yy} = [\mathbb{D}]_{22} = D_X \sin^2\theta + D_Y \cos^2\theta$. For the rest of the paper we take U, D_X, D_Y, and D_θ to be constants, so that Eq. (3.9) simplifies to

$$\partial_t \bar{p} = -U \sin\theta \, \partial_y \bar{p} + D_{yy}(\theta) \, \partial_y^2 \bar{p} + D_\theta \, \partial_\theta^2 \bar{p}. \tag{3.10}$$

(Note that instead of defining $\bar{p}$ as in (3.8) we could assume that p is independent of x, in which case p is a density per unit length that satisfies (3.10).) Equation (3.10) is our main focus. The corresponding flux vector (3.6) reduces to

$$\bar{\boldsymbol{f}} = (U \sin\theta \, \bar{p} - D_{yy}(\theta) \, \partial_y \bar{p}) \, \hat{\boldsymbol{y}} - D_\theta \, \partial_\theta \bar{p} \, \hat{\boldsymbol{\theta}}. \tag{3.11}$$

For the channel geometry, the domain can be characterized by $\zeta_-(\theta) < y < \zeta_+(\theta)$, so the normal vector is

$$\bar{\boldsymbol{n}} = \zeta'_\pm(\theta) \, \hat{\boldsymbol{\theta}} - \hat{\boldsymbol{y}}. \tag{3.12}$$

The no-flux boundary conditions on Eq. (3.10) comes from (3.7):

$$\bar{\boldsymbol{f}} \cdot \bar{\boldsymbol{n}} = -(U \sin\theta \, \bar{p} - D_{yy}(\theta) \, \partial_y \bar{p}) - \zeta'_\pm(\theta) \, D_\theta \, \partial_\theta \bar{p} = 0, \qquad y = \zeta_\pm(\theta). \tag{3.13}$$

For convenience, we gather together the main Eq. (3.10) and its no-flux boundary condition (3.13) for an infinite channel geometry:

$$\partial_t \bar{p} + U \sin\theta \, \partial_y \bar{p} - D_{yy}(\theta) \, \partial_y^2 \bar{p} - D_\theta \, \partial_\theta^2 \bar{p} = 0, \qquad \zeta_-(\theta) < y < \zeta_+(\theta); \tag{3.14a}$$

$$U \sin\theta \, \bar{p} - D_{yy}(\theta) \, \partial_y \bar{p} + \zeta'_\pm(\theta) \, D_\theta \, \partial_\theta \bar{p} = 0, \qquad y = \zeta_\pm(\theta). \tag{3.14b}$$

As discussed in Section 2, the domain in θ is $[-\pi, \pi]$ (periodic) for $\zeta_-(\theta) < \zeta_+(\theta)$, which means the swimmer can fully reverse direction in the channel (open channel configuration, Fig. 5a). If $\zeta_-(\theta) \le \zeta_+(\theta)$, the domain 'pinches off' whenever $\zeta_-(\theta) = \zeta_+(\theta)$, and consists of two or more disconnected pieces (closed channel configuration, Fig. 5b).

4. Reduced equation

Equation (3.14) is a challenging equation to solve, in particular because of the complicated boundary shape. We can dramatically simplify the problem by assuming that the diffusivity D_θ is small, and carrying out an expansion in powers of $\varepsilon = D_\theta$. We call this the small-D_θ or *reduced* limit. The reduced form of Eq. (3.14), given by Eq. (4.15), will enable us to solve for the invariant density for a swimmer in Section 5, as well as many other quantities of interest such as a swimmer's mean reversal time (Section 6) and its effective diffusivity along the channel (Section 7).

Take Eq. (3.14) and write $D_\theta = \varepsilon$:

$$U \sin\theta\, \partial_y \bar{p} - D_{yy}(\theta)\, \partial_y^2 \bar{p} = \varepsilon\, (\partial_\theta^2 \bar{p} - \partial_T \bar{p}), \qquad \zeta_-(\theta) < y < \zeta_+(\theta); \tag{4.1a}$$

$$U \sin\theta\, \bar{p} - D_{yy}(\theta)\, \partial_y \bar{p} = -\varepsilon\, \zeta'_\pm(\theta)\, \partial_\theta \bar{p}, \qquad y = \zeta_\pm(\theta), \tag{4.1b}$$

where we also defined a slow time $T = \varepsilon t$, $\partial_t \to \varepsilon\, \partial_T$. We write the regular expansion

$$\bar{p}(\theta, y, T) = \bar{p}_0(\theta, y, T) + \varepsilon\, \bar{p}_1(\theta, y, T) + \varepsilon^2\, \bar{p}_2(\theta, y, T) + \dots \tag{4.2}$$

and proceed to solve for $\bar{p}_i$ order-by-order.

At order ε^0, Eq. (4.1) is

$$U \sin\theta\, \partial_y \bar{p}_0 - D_{yy}(\theta)\, \partial_y^2 \bar{p}_0 = 0, \qquad U \sin\theta\, \bar{p}_0 - D_{yy}(\theta)\, \partial_y \bar{p}_0 = 0, \quad y = \zeta_\pm(\theta) \tag{4.3}$$

with solution

$$\bar{p}_0(\theta, y) = Q(\theta, T)\, \mathrm{e}^{\sigma(\theta)\, y}, \qquad \sigma(\theta) := U \sin\theta / D_{yy}(\theta), \tag{4.4}$$

where $Q(\theta, T)$ is as-yet undetermined.

At order ε^1, Eq. (4.1) is

$$U \sin\theta\, \partial_y \bar{p}_1 - D_{yy}(\theta)\, \partial_y^2 \bar{p}_1 = \partial_\theta^2 \bar{p}_0 - \partial_T \bar{p}_0; \tag{4.5a}$$

$$U \sin\theta\, \bar{p}_1 - D_{yy}(\theta)\, \partial_y \bar{p}_1 = -\zeta'_\pm(\theta)\, \partial_\theta \bar{p}_0, \quad y = \zeta_\pm(\theta). \tag{4.5b}$$

Integrate Eq. (4.5a) from $y = \zeta_-$ to ζ_+ and use the boundary conditions (4.5b) to get on the left

$$\int_{\zeta_-(\theta)}^{\zeta_+(\theta)} (U \sin\theta\, \partial_y \bar{p}_1 - D_{yy}\, \partial_y^2 \bar{p}_1)\, \mathrm{d}y = [U \sin\theta\, \bar{p}_1 - D_{yy}(\theta)\, \partial_y \bar{p}_1]_{\zeta_-(\theta)}^{\zeta_+(\theta)}$$

$$= -\zeta'_+(\theta)\, \partial_\theta \bar{p}_0(\theta, \zeta_+(\theta)) + \zeta'_-(\theta)\, \partial_\theta \bar{p}_0(\theta, \zeta_-(\theta)).$$

On the right, the integral of the term $\partial_\theta^2 \bar{p}_0$ is

$$\int_{\zeta_-(\theta)}^{\zeta_+(\theta)} \partial_\theta^2 \bar{p}_0\, \mathrm{d}y = \partial_\theta \int_{\zeta_-(\theta)}^{\zeta_+(\theta)} \partial_\theta \bar{p}_0\, \mathrm{d}y - \zeta'_+(\theta)\, \partial_\theta \bar{p}_0(\theta, \zeta_+(\theta)) + \zeta'_-(\theta)\, \partial_\theta \bar{p}_0(\theta, \zeta_-(\theta)).$$

Combining the last two equations, we obtain

$$\partial_T \int_{\zeta_-(\theta)}^{\zeta_+(\theta)} \bar{p}_0\, \mathrm{d}y = \partial_\theta \int_{\zeta_-(\theta)}^{\zeta_+(\theta)} \partial_\theta \bar{p}_0\, \mathrm{d}y. \tag{4.6}$$

We can then carry out the y integral on the right of (4.6) after using Eq. (4.4), to get

$$\int_{\zeta_-(\theta)}^{\zeta_+(\theta)} (\partial_\theta Q + \sigma'(\theta) Q\, y) \mathrm{e}^{\sigma(\theta)\, y}\, \mathrm{d}y = w(\theta)\, \partial_\theta Q - \nu(\theta) Q \tag{4.7a}$$

where we defined the weight

$$
\begin{aligned}
w(\theta) &= \int_{\zeta_-(\theta)}^{\zeta_+(\theta)} e^{\sigma(\theta)\,y}\,\mathrm{d}y \\
&= \left(e^{\sigma(\theta)\,\zeta_+(\theta)} - e^{\sigma(\theta)\,\zeta_-(\theta)}\right)/\sigma(\theta),
\end{aligned}
\tag{4.8a}
$$

and the drift

$$
\begin{aligned}
\nu(\theta) &= -\sigma'(\theta) \int_{\zeta_-(\theta)}^{\zeta_+(\theta)} y\, e^{\sigma(\theta)\,y}\,\mathrm{d}y \\
&= -\frac{\sigma'(\theta)}{\sigma(\theta)}\left(\left[y\,e^{\sigma(\theta)\,y}\right]_{\zeta_-(\theta)}^{\zeta_+(\theta)} - \int_{\zeta_-(\theta)}^{\zeta_+(\theta)} e^{\sigma(\theta)\,y}\,\mathrm{d}y\right) \\
&= \frac{\sigma'(\theta)}{\sigma(\theta)}\left(w(\theta) - e^{\sigma(\theta)\,\zeta_+(\theta)}\,\zeta_+(\theta) + e^{\sigma(\theta)\,\zeta_-(\theta)}\,\zeta_-(\theta)\right).
\end{aligned}
\tag{4.8b}
$$

Note that $w(\theta) > 0$ if $\zeta_+(\theta) > \zeta_-(\theta)$, and $w(\theta) = 0$ if and only if $\zeta_+(\theta) = \zeta_-(\theta)$. Thus, $w(\theta)$ only vanishes when the domain "pinches off," as described in Section 2.2.2. Despite the apparent singularity, the weight w is nonsingular when σ is small:

$$
w(\theta) \sim \zeta_+(\theta) - \zeta_-(\theta), \qquad \sigma \to 0.
\tag{4.9}
$$

Another convenient form for the drift ν is

$$
\nu(\theta) = w(\theta)\frac{\sigma'(\theta)}{\sigma(\theta)}\left[1 - \frac{\sigma(\theta)}{2\sinh\Delta(\theta)}\left(e^{\Delta(\theta)}\,\zeta_+(\theta) - e^{-\Delta(\theta)}\,\zeta_-(\theta)\right)\right]
\tag{4.10}
$$

with

$$
\Delta(\theta) := \tfrac{1}{2}\sigma(\theta)\,(\zeta_+(\theta) - \zeta_-(\theta)).
\tag{4.11}
$$

The function ν appears singular as $\Delta \to 0$, but the limit exists:

$$
\frac{\nu(\theta)}{w(\theta)} \sim -\tfrac{1}{2}\sigma'(\theta)(\zeta_+(\theta) + \zeta_-(\theta)), \qquad \Delta \to 0.
\tag{4.12}
$$

This expression is valid whether Δ vanishes owing to $\sigma(\theta) = 0$ or $\zeta_+(\theta) = \zeta_-(\theta)$.

Doing the y integral on the left of (4.6), we finally obtain the reduced equation

$$
w(\theta)\,\partial_T Q + \partial_\theta(\nu(\theta)Q - w(\theta)\,\partial_\theta Q) = 0.
\tag{4.13}
$$

The reduced equation is a $(1+1)$-dimensional drift-diffusion PDE that captures the time-evolution of the marginal probability density

$$
P(\theta,T) = \int_{\zeta_-(\theta)}^{\zeta_+(\theta)} \bar{p}_0(\theta,y,T)\,\mathrm{d}y = w(\theta)\,Q(\theta,T).
\tag{4.14}
$$

The weight function $w(\theta)$ and drift $\nu(\theta)$ encode the effect of the shape of the configuration space.

We can transform (4.13) into an equation for P:

$$\partial_T P + \partial_\theta(\mu(\theta)\, P - \partial_\theta P) = 0, \tag{4.15}$$

with

$$w(\theta)\,\mu(\theta) := \nu(\theta) + w'(\theta) = e^{\sigma(\theta)\,\zeta_+(\theta)}\zeta'_+(\theta) - e^{\sigma(\theta)\,\zeta_-(\theta)}\zeta'_-(\theta). \tag{4.16}$$

An explicit form for μ in terms of Δ in (4.11) is

$$\mu(\theta) = \frac{\sigma(\theta)}{2\sinh\Delta(\theta)}\left(e^{\Delta(\theta)}\,\zeta'_+(\theta) - e^{-\Delta(\theta)}\,\zeta'_-(\theta)\right). \tag{4.17}$$

Though Eq. (4.15) is slightly nicer than Eq. (4.13), it has the disadvantage that it requires a derivative $w'(\theta)$ in $\mu(\theta)$, which can cause problems for nonsmooth swimmer shapes.

Example 4 ($\mu(\theta)$ for elliptical and needle swimmers)**.** For the elliptical swimmer described by Eq. (2.16), we have

$$\mu_{\mathrm{ellipse}}(\theta) = -\tfrac{1}{2}e^2\,\frac{a\sigma(\theta)\sin 2\theta}{\sqrt{1 - e^2\cos^2\theta}}\coth\Delta(\theta) + X_{\mathrm{rot}}\,\sigma(\theta)\cos\theta \tag{4.18}$$

with $\Delta(\theta) = \tfrac{1}{2}\sigma(\theta)(L - 2a\sqrt{1 - e^2\cos^2\theta})$. Note that μ vanishes when $e = 0$ (circular or point swimmer). The needle is the limit of (4.18) as $e \to 1$:

$$\mu_{\mathrm{needle}}(\theta) = -a\sigma(\theta)\cos\theta\,\mathrm{sgn}\,\theta\coth\Delta(\theta) + X_{\mathrm{rot}}\,\sigma(\theta)\cos\theta. \tag{4.19}$$

These are plotted in Fig. 6. Note that $\mu_{\mathrm{needle}}(\theta)$ is discontinuous at $\theta = 0$, due to the singular derivative of w in (4.16). $\triangle$

5. Invariant density

A natural quantity to compute from the reduced equation (4.13) is the *invariant density* for the swimmer. This is the time-independent solution $Q(\theta, T) = \mathcal{Q}(\theta)$ to (4.13):

$$\frac{d}{d\theta}\left(\nu(\theta)\,\mathcal{Q}(\theta) - w(\theta)\,\mathcal{Q}'(\theta)\right) = 0. \tag{5.1}$$

$\mathcal{Q}$ is unique for a periodic domain Ω or a single component Ω_i; see Section 2.2. Note that $\mathcal{Q}$ (and hence the invariant density) is independent of D_θ at leading order.

To find the invariant density, we first integrate Eq. (5.1) once to get

$$\nu(\theta)\,\mathcal{Q}(\theta) - w(\theta)\,\mathcal{Q}'(\theta) = c_2\,. \tag{5.2}$$

The solution to (5.2) then can be written

$$\mathcal{Q}(\theta) = c_1\,(1 - c_2\,F(\theta))\,e^{\Phi(\theta)} \tag{5.3}$$
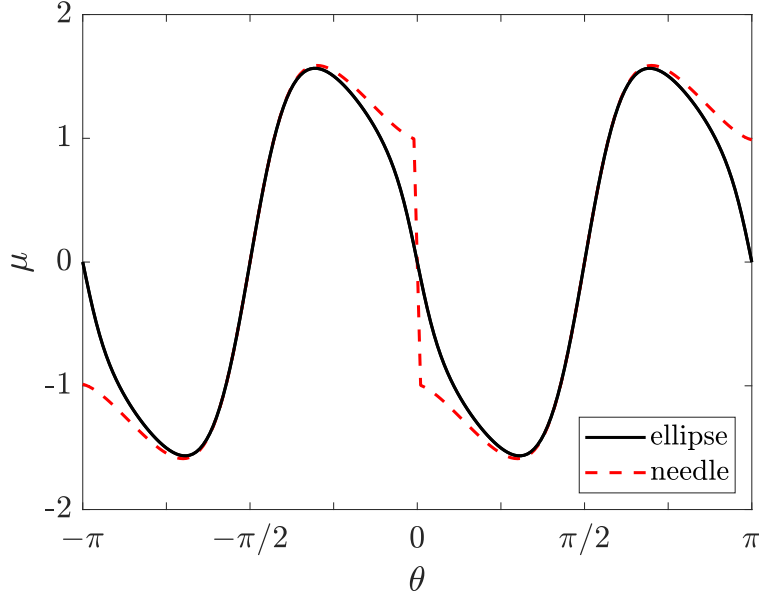
FIGURE 6. The angular drift $\mu_{\text{ellipse}}(\theta)$ (Eq. (4.18)) in a channel of width $L = 1.2$ for an ellipse with $a = 1/2$, $b = 1/8$, $U = D_X = D_Y = 1$, $X_{\text{rot}} = -1/4$. The dashed line is $\mu_{\text{needle}}(\theta)$ ($b = 0$, Eq. (4.19)).

where

$$\Phi(\theta) := \int_{\theta^{\text{L}}}^{\theta} \frac{\nu(\vartheta)}{w(\vartheta)} \, \mathrm{d}\vartheta, \qquad F(\theta) := \int_{\theta^{\text{L}}}^{\theta} \frac{\mathrm{d}\vartheta}{c_1 w(\vartheta) \, \mathrm{e}^{\Phi(\vartheta)}} \tag{5.4}$$

and θ^{L} is the leftmost domain limit ($\theta^{\text{L}} = -\pi$ for Ω and $\theta^{\text{L}} = \theta_i^{\text{L}}$ for Ω_i; see Section 2.2). The integrand in (5.4) appears singular as $\Delta \to 0$, but the limit exists as we saw in Eq. (4.12).

Next we need to determine the constants c_1 and c_2. Normalization of $\mathcal{P} := w\mathcal{Q}$ determines c_1, but c_2 depends on whether we have an open or closed channel configuration space (Section 2.2). We treat these two cases separately.

5.1. **Open channel.** For the open channel configuration space as described in Section 2.2.1, $w(\theta)$ and $\nu(\theta)$ are 2π-periodic. The boundary condition on $\mathcal{Q}(\theta)$ is that it be periodic as well. Choosing $\theta^{\text{L}} = -\pi$ in Eq. (5.4), we have

$$\mathcal{Q}(-\pi) = c_1 = \mathcal{Q}(\pi) = c_1 \left(1 - c_2 \, F(\pi)\right) \mathrm{e}^{\Phi(\pi)}. \tag{5.5}$$

We solve for c_2 in Eq. (5.5) to obtain

$$c_2 = \left(1 - \mathrm{e}^{-\Phi(\pi)}\right)/F(\pi) \tag{5.6}$$

and

$$\mathcal{Q}(\theta) = c_1 \, \mathrm{e}^{\Phi(\theta)} \big(1 - \big(1 - \mathrm{e}^{-\Phi(\pi)} \big) F(\theta)/F(\pi) \big). \tag{5.7}$$

The constant c_1 is chosen to enforce the normalization of $\mathcal{P} = w\mathcal{Q}$:

$$\int_{-\pi}^{\pi} \int_{\zeta_-(\theta)}^{\zeta_+(\theta)} \bar{p}_0(\theta, y) \, \mathrm{d}y \, \mathrm{d}\theta = \int_{-\pi}^{\pi} \mathcal{P}(\theta) \, \mathrm{d}\theta = 1. \tag{5.8}$$

If $\Phi(\theta)$ happens to be 2π-periodic, then we have $\Phi(\pi) = 0$, so $c_2 = 0$ and

$$\mathcal{Q}(\theta) = c_1 \, \mathrm{e}^{\Phi(\theta)}, \qquad (\Phi(\theta) \ 2\pi\text{-periodic}). \tag{5.9}$$

The invariant probability density in this case satisfies *detailed balance* [79]. In fact $\Phi(\theta)$ is periodic for the very important case of a left-right symmetric swimmer, for then we have $\zeta_+(\theta) = -\zeta_-(-\theta)$, which follows from symmetries (2.18) and (2.21). This leads to $\Delta(-\theta) = -\Delta(\theta)$ and the integrand of Eq. (5.4) is odd in θ. Choosing $\theta^{\mathrm{L}} = -\pi$ then gives $\Phi(-\pi) = \Phi(\pi) = 0$, *i.e.*, Φ is periodic.

From $\mathcal{Q}$, we can reconstruct the full invariant density from Eq. (4.4) as $\bar{p}_0(\theta, y) = \mathcal{Q}(\theta) \, \mathrm{e}^{\sigma(\theta)y}$, with $\sigma(\theta) = U \sin\theta / D_{yy}(\theta)$. The exponential term reflects the accumulation near both walls, as observed in experiments and simulations. The thickness of the boundary layer is $D_{yy}/U \sin\theta$, which agrees qualitatively with the results for a spherical swimmer in [23, 29]. A typical invariant density in an open-channel configuration is shown in Fig. 7a for a needle swimmer. The marginal invariant probability density $\mathcal{P}(\theta)$ is plotted in Fig. 8a for elliptical swimmers with different velocities U and centers of rotation X_{rot}. From Fig. 7, the invariant marginal density in y peaks near both walls, but not exactly at the walls, in accordance with the simulations in the appendix of [29].

What is the meaning of nonzero c_2? It represents an average rotational drift of the needle's stochastic angle $\theta(t)$. To see this, note that in the equilibrium state, we have the expectation

$$\mathbb{E}\mu(\theta(T)) = \int_{-\pi}^{\pi} \mu(\theta) \, \mathcal{P}(\theta) \, \mathrm{d}\theta = \int_{-\pi}^{\pi} (\mathcal{P}'(\theta) + c_2) \, \mathrm{d}\theta = 2\pi c_2 \tag{5.10}$$

since $\mu\mathcal{P} - \mathcal{P}' = c_2$ and $\mathcal{P}(\theta)$ is periodic. Hence, the average rate of angular rotation of the swimmer is $\omega = 2\pi c_2$. From (5.4), the periodic average of $\mu(\theta)$ is

$$\bar{\mu} = \frac{1}{2\pi} \int_{-\pi}^{\pi} \mu(\theta) \, \mathrm{d}\theta = \frac{1}{2\pi} \int_{-\pi}^{\pi} \frac{\nu(\theta)}{w(\theta)} \, \mathrm{d}\theta = \frac{\Phi(\pi)}{2\pi} = \frac{1}{2\pi} \log(1 - c_2 F(\pi))^{-1} \tag{5.11}$$

which is zero if and only if $c_2 = 0$ (Eq. (5.6)).

Example 5 (invariant density for fast needle swimmer)**.** It is in general quite challenging to get closed-form solutions for the invariant density of a swimmer, but
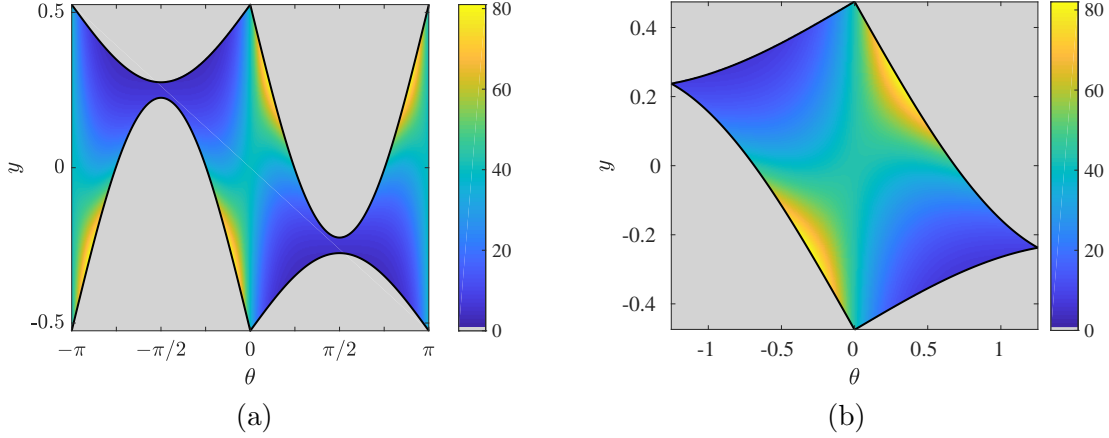
FIGURE 7. Invariant density $\bar{p}_0 = \mathcal{Q}(\theta)\,\mathrm{e}^{\sigma(\theta)\,y}$ for $U = 1$ and $D_X = D_Y = 0.1$ for the needle in Fig. 4b of length $\ell = 2a = 1$ in (a) an open channel of width $L = 1.05$; (b) a closed channel of width $L = 0.95$, for the domain Ω_1 in Fig. 5b.
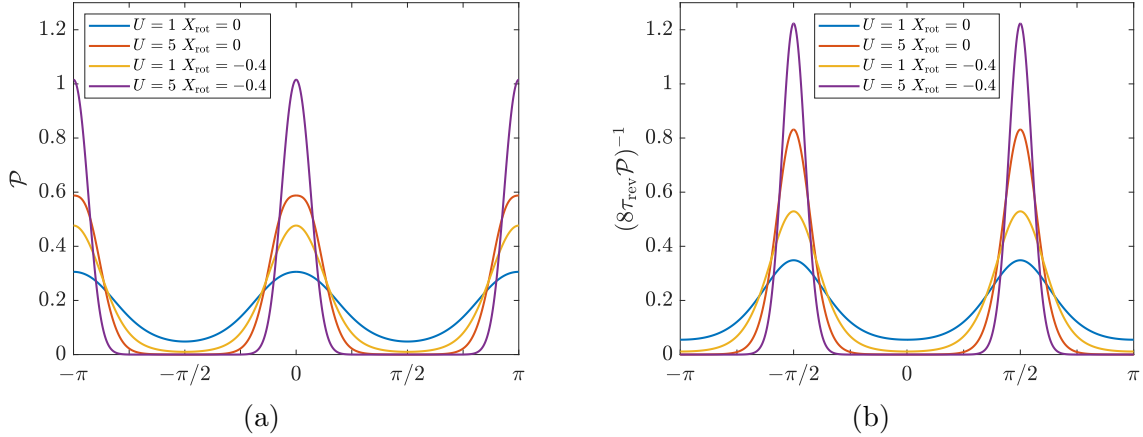
FIGURE 8. For an ellipse with $2a = b = 1$, $D_X = D_Y = 0.1$, $D_\theta = 0.01$, $U = 1$, in a channel of width $L = 1.2$: (a) Marginal invariant probability density $\mathcal{P}(\theta)$; (b) $1/\mathcal{P}$, normalized to unit area (see Eq. (6.8) for definition of τ_{rev}).

it can be done in the large-U limit. From Eqs. (4.16) and (5.4) we have

$$\Phi(\theta) = \int_{-\pi}^{\theta} \mu(\vartheta)\,\mathrm{d}\vartheta - \log w(\theta) + \text{const.,} \tag{5.12}$$

and so the leading-order invariant marginal density $\mathcal{P} = c_1 w\, \mathrm{e}^\Phi$ for a left-right symmetric swimmer is

$$\mathcal{P}(\theta) = \bar{c}_1 \, \exp\!\left(\int_{-\pi}^{\theta} \mu(\vartheta)\, \mathrm{d}\vartheta \right) \tag{5.13}$$

with $\bar{c}_1$ a normalization constant. For large U, the constant $\bar{c}_1$ can be determined by approximating the normalization integral using the maxima of μ.

We illustrate this here for the needle swimmer of Examples 1 and 4. For large U, we can approximate $\coth \Delta \approx \mathrm{sgn}(\theta)$ for $\mu = \mu_{\mathrm{needle}}$ in Eq. (4.19), and we have

$$\mu(\theta) \approx -\sigma(\theta) \cos\theta \, (a - X_{\mathrm{rot}}), \qquad U \to \infty, \tag{5.14}$$

with σ defined in Eq. (4.4), and $a = \ell/2$ the needle half-length. Note that the channel width L does not appear in (5.14) at leading order in large U: the needle spends most of its time stuck to one of the walls, so the channel width is not important. We can integrate (5.14) and use the result in (5.13) to find

$$\mathcal{P}(\theta) = \bar{c}_1 \exp\!\left(\beta \, \log\!\left(\alpha \sin^2\theta + \cos^2\theta \right)^{1/(1-\alpha)} \right), \tag{5.15}$$

with

$$\alpha := D_X/D_Y, \qquad \beta := U(a - X_{\mathrm{rot}})/2D_Y \gg 1. \tag{5.16}$$

We can see that "large U" in nondimensional terms means large β, which is a Péclet number that accounts for the position of the center of rotation: β is maximized when the center of rotation is at the rear ($X_{\mathrm{rot}} = -a$), which is a pusher-like swimmer. We can now use Laplace's method to find the normalization constant $\bar{c}_1$. The maxima of the argument of the exponential in (5.15) correspond to the zeros of μ at $\theta = 0$ and π (with $-a \leq X_{\mathrm{rot}} < a$). We thus find

$$\mathcal{P}(\theta) = \sqrt{\frac{\beta}{4\pi}} \left(\alpha \sin^2\theta + \cos^2\theta \right)^{\beta/(1-\alpha)}, \qquad \beta \gg 1. \tag{5.17}$$

In the limit $\alpha = 1$ (equal diffusivities), Eq. (5.17) simplifies to

$$\mathcal{P}(\theta) = \sqrt{\frac{\beta}{4\pi}} \, \mathrm{e}^{-\beta \sin^2\theta}, \qquad \beta \gg 1. \tag{5.18}$$

Note that the limit $\alpha \to 0$ in (5.17) is well-defined and gives $\mathcal{P}(\theta) = \sqrt{\beta/4\pi}\, |\cos\theta|^{2\beta}$. However, the limit $\alpha \to \infty$ gives an improperly normalized density, indicating that the limits $\beta, \alpha \to \infty$ do not commute. (The quartic term in a Taylor series expansion of the log in (5.15) has coefficient proportional to α, and cannot be neglected when applying Laplace's method.)

In Fig. 9 we compare a numerical solution for $\mathcal{P}$ to the large-U form (5.17). There is some discrepancy near $\theta = 0, \pi$, which comes from the approximation (5.14) breaking down near those points, but the difference vanishes as U gets larger. We also
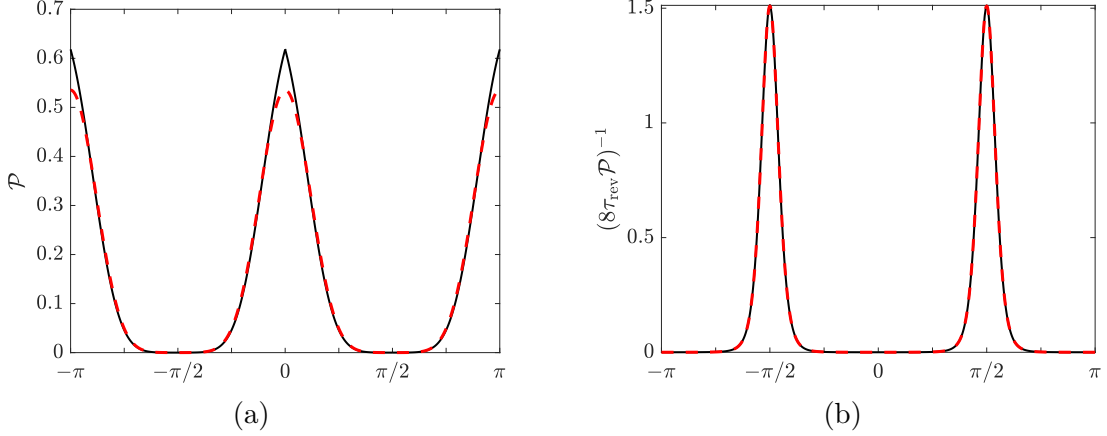
FIGURE 9. For a needle with $\ell = 1$, $U = 8$, $D_X = 0.1$, $D_Y = 1$, $D_\theta = 0.01$, in a channel of width $L = 1.2$ ($\beta = 3.6$): (a) Marginal invariant probability density $\mathcal{P}(\theta)$ (solid) and large-U form (5.17) (dashed). Notice the discrepancy near $\theta = 0, \pi$, which goes away for large U. (b) $1/\mathcal{P}$, normalized to unit area, for the same parameters.

plot $1/\mathcal{P}$, which we shall need in Section 6, for which the approximation is uniformly much better.

$\triangle$

Example 6 (invariant density for fast circular swimmer). When the swimmer is perfectly circular, putting $e = 0$ in Eq. (4.18) gives $\mu(\theta) = X_{\mathrm{rot}}\,\sigma(\theta)\cos\theta$, which is the same as (5.14) with $a = 0$ in the previous example, except that here this expression is exact. The invariant density thus has the form (5.15), with $\beta = -UX_{\mathrm{rot}}/2D_Y$, which can have either sign. For $\beta > 0$ and large we recover Eqs. (5.17) and (5.18) — the circular swimmer tends to align parallel to the wall. For $-\beta > 0$ and large the maxima of $\int \mu\,d\theta$ switch from $\{0, \pi\}$ to $\pm\pi/2$, and we get instead of Eq. (5.17):

$$\mathcal{P}(\theta) = \sqrt{\frac{|\beta|}{4\pi\alpha}} \left(\sin^2\theta + \alpha^{-1}\cos^2\theta\right)^{-|\beta|/(1-\alpha)}, \qquad -\beta \gg 1, \qquad (5.19)$$

which for $\alpha = 1$ simplifies to

$$\mathcal{P}(\theta) = \sqrt{\frac{|\beta|}{4\pi}}\, \mathrm{e}^{-|\beta|\cos^2\theta}, \qquad -\beta \gg 1. \qquad (5.20)$$

Comparing the latter to (5.18), we can see that puller-like circular swimmers ($X_{\mathrm{rot}} > 0$) collect at $\theta = \pm\pi/2$, swimming towards the wall, rather than aligning parallel to the wall. The limit $\alpha \to 0$ in 5.19 gives $\mathcal{P}(\theta) = \frac{1}{2}(\delta(\theta - \pi/2) + \delta(\theta + \pi/2))$. $\triangle$

5.2. **Closed channel.** For a closed channel configuration space, as described in Section 2.2.2, the domain is given by Ω_i in Eq. (2.25), for some fixed i. Now the boundary condition is that there be no net flux in the θ direction, so the constant $c_2 = 0$ in Eq. (5.2). The solution for the invariant density is thus

$$\mathcal{Q}(\theta) = c_1 \, \mathrm{e}^{\Phi(\theta)}, \qquad \theta_i^{\mathrm{L}} \le \theta \le \theta_i^{\mathrm{R}}, \tag{5.21}$$

with c_1 obtained by the normalization condition for $\mathcal{P} = w\mathcal{Q}$:

$$\int_{\theta_i^{\mathrm{L}}}^{\theta_i^{\mathrm{R}}} \int_{\zeta_-(\theta)}^{\zeta_+(\theta)} \bar{p}_0(\theta, y) \, \mathrm{d}y \, \mathrm{d}\theta = \int_{\theta_i^{\mathrm{L}}}^{\theta_i^{\mathrm{R}}} \mathcal{P}(\theta) \, \mathrm{d}\theta = 1. \tag{5.22}$$

A typical invariant density in a closed-channel configuration is shown in Fig. 7b for a needle swimmer.

6. Mean exit and mean reversal times

A standard problem in drift-diffusion processes is to compute the *mean exit time* (MET) of a particle to some exit, also called a first-passage time [32, 37, 47, 69, 82, 117]. Associated with the reduced drift-diffusion equation (4.15) is a reduced equation for the mean exit time $\tau(\theta)$:

$$\mu(\theta) \, \tau' + \tau'' = -1, \qquad \theta^{\mathrm{L}} < \theta < \theta^{\mathrm{R}}; \tag{6.1a}$$

$$\tau(\theta^{\mathrm{L}}) = \tau(\theta^{\mathrm{R}}) = 0. \tag{6.1b}$$

The left-hand side of (6.1a) is the adjoint of the linear operator in Eq. (4.15) [37, 47, 82]. The solution to Equation (6.1) gives the expected time τ for a particle starting at θ (for any y) to reach an 'exit' at $\theta = \theta^{\mathrm{L}}$ or $\theta = \theta^{\mathrm{R}}$. Note that since $T = D_\theta t$ in Eq. (4.15) the dimensional MET is τ/D_θ, which goes to infinity as $D_\theta \to 0$, *i.e.*, the exit cannot be reached if $D_\theta = 0$. The word exit here is interpreted loosely: the MET merely signifies the first time a swimmer's orientation achieves the value θ^{L} or θ^{R}, starting from some value θ.

6.1. **Solving the mean exit time equation.** To solve Eq. (6.1), define $\mathrm{T} = w\tau'$ which satisfies

$$(\nu/w) \, \mathrm{T} + \mathrm{T}' = -w, \qquad \mathrm{T} = w\tau', \tag{6.2}$$

where $w(\theta)$ and $\nu(\theta)$ are defined in (4.8). Use the integrating factor $\tilde{c}_1 \, \mathrm{e}^{\Phi(\theta)}$ from Eq. (5.4) to get

$$\tau'(\theta) = -\frac{1}{\widetilde{\mathcal{P}}(\theta)} \Big(\widetilde{G}(\theta) - \mathcal{C} \Big), \qquad \widetilde{G}(\theta) := \int_{\theta^{\mathrm{L}}}^{\theta} \widetilde{\mathcal{P}}(\vartheta) \, \mathrm{d}\vartheta, \tag{6.3}$$

where $\widetilde{\mathcal{P}}(\theta) = \tilde{c}_1 \, w \, e^{\Phi}$ is analogous to the invariant density for a closed channel (5.21) and $\mathcal{C}$ is an integration constant. We choose $\tilde{c}_1$ so that the normalization condition (5.22) is satisfied: $\widetilde{G}(\theta^{\mathrm{R}}) = 1$; hence, $\widetilde{G}(\theta)$ is the equilibrium probability of finding the swimmer between θ^{L} and θ, *if* the channel were closed. The mean exit time τ has a unique maximum at $\theta = \theta_*$ with $\mathcal{C} = \widetilde{G}(\theta_*)$.

Now integrate Eq. (6.3):

$$\tau(\theta) = \int_{\theta^{\mathrm{L}}}^{\theta} \frac{1}{\widetilde{\mathcal{P}}(\vartheta)} \left(\mathcal{C} - \widetilde{G}(\vartheta) \right) \mathrm{d}\vartheta, \tag{6.4}$$

which satisfies the left boundary condition $\tau(\theta^{\mathrm{L}}) = 0$. The right boundary condition then requires $\tau(\theta^{\mathrm{R}}) = 0$, which fixes the integration constant

$$\mathcal{C} = \int_{\theta^{\mathrm{L}}}^{\theta^{\mathrm{R}}} \frac{\widetilde{G}(\vartheta)}{\widetilde{\mathcal{P}}(\vartheta)} \, \mathrm{d}\vartheta \Big/ \int_{\theta^{\mathrm{L}}}^{\theta^{\mathrm{R}}} \frac{\mathrm{d}\vartheta}{\widetilde{\mathcal{P}}(\vartheta)}. \tag{6.5}$$

Equations (6.4) and (6.5) give the mean exit time for a swimmer starting at θ and exiting at either θ^{L} or θ^{R}. We now focus on a particular version of this mean exit time with a more natural interpretation — the mean reversal time.

6.2. **Mean reversal time.** The *mean reversal time* τ_{rev} (or turnaround time [37]) is the expected time for a swimmer initially oriented with $\theta = 0$ to reverse direction to $\theta = \pm\pi$. It can be obtained from Eq. (6.4) by setting $-\theta^{\mathrm{L}} = \theta^{\mathrm{R}} = \pi$ and $\theta = 0$:

$$\tau_{\mathrm{rev}} = \tau(0) = \int_{-\pi}^{0} \frac{1}{\widetilde{\mathcal{P}}(\vartheta)} \left(\mathcal{C} - \widetilde{G}(\vartheta) \right) \mathrm{d}\vartheta. \tag{6.6}$$

In Appendix A we show how the constant $\mathcal{C}$ can be eliminated to obtain

$$\tau_{\mathrm{rev}} = \frac{\widetilde{G}(0)}{1 + e^{\pi\bar{\mu}}} \int_{-\pi}^{0} \frac{\mathrm{d}\vartheta}{\widetilde{\mathcal{P}}(\vartheta)} + \tanh(\pi\bar{\mu}/2) \int_{-\pi}^{0} \frac{\widetilde{G}(\vartheta)}{\widetilde{\mathcal{P}}(\vartheta)} \, \mathrm{d}\vartheta \tag{6.7}$$

where $\bar{\mu}$ is defined in (5.11). For a left-right symmetric swimmer, $\widetilde{\mathcal{P}} = \mathcal{P}$, $\bar{\mu} = 0$, and $\widetilde{G}(0) = 1/2$ by symmetry, so we obtain the compact expression

$$\tau_{\mathrm{rev}} = \tfrac{1}{4} \int_{0}^{\pi} \frac{\mathrm{d}\theta}{\mathcal{P}(\theta)}. \tag{6.8}$$

Example 7 (mean reversal time with diffusion only). In the absence of swimming ($U = 0$), we have $\nu = 0$ from Eq. (4.8b), and $\widetilde{\mathcal{P}} = \mathcal{P} = c_1 w$, with $c_1^{-1} = \int_{-\pi}^{\pi} w \, \mathrm{d}\theta$. Hence, Eq. (6.8) is

$$\tau_{\mathrm{rev}} = \frac{1}{2} \left(\int_{0}^{\pi} w(\theta) \, \mathrm{d}\theta \right) \left(\int_{0}^{\pi} \frac{\mathrm{d}\theta}{w(\theta)} \right). \tag{6.9}$$

For a needle with wall distance function (2.8), we get from Eq. (2.20)

$$w(\theta) = \zeta_+(\theta) - \zeta_-(\theta) = L - \ell \, |\sin \theta| \tag{6.10}$$

where $X_{\rm rot}$ drops out: the center of rotation is immaterial in the absence of swimming. We can then easily compute the integral (6.9) to obtain

$$\tau_{\rm rev} = \frac{(\pi - 2\lambda)(\pi - \arccos \lambda)}{\sqrt{1 - \lambda^2}}, \qquad \lambda := \ell/L < 1. \tag{6.11}$$

The 'narrow exit' limit corresponds to $\lambda = 1 - \delta$, with δ small.

$$\tau_{\rm rev} = \frac{\pi(\pi - 2)}{\sqrt{2\delta}} + O(\delta^0), \qquad \delta \ll 1. \tag{6.12}$$

This is similar but not identical to Holcman & Schuss's result [37, Eq. (5.13)]:

$$\tau_{\rm rev} = \frac{\pi(\pi - 2)}{\sqrt{2\delta}} \sqrt{\frac{D_Y}{2L^2 D_\theta}} \tag{6.13}$$

valid as $\delta \to 0$, but otherwise unconstrained. In Fig. 10, a comparison to a finite-element numerical solution of the full PDE (*i.e.*, without using the reduced equation) shows excellent agreement with our small-D_θ form (6.11), but less so with the form (6.13). Possibly there is a parameter regime where (6.13) shows better agreement.

For an elliptical shape (2.16) with $U = 0$, we have

$$w(\theta) = L \left(1 - \lambda\sqrt{1 - e^2 \cos^2 \theta}\right). \tag{6.14}$$

Then

$$L^{-1} \int_0^\pi w(\theta) \, \mathrm{d}\theta = \pi - 2\lambda E(e), \tag{6.15}$$

where E is a complete elliptic integrals of the second kind. We also have

$$\int_0^\pi \frac{L \, \mathrm{d}\theta}{w(\theta)} = \frac{\pi}{\sqrt{(1 - \lambda^2)(1 - (1 - e^2)\lambda^2)}} - \frac{2}{\lambda} K(e) + \frac{2}{\lambda(1 - \lambda^2)} \Pi\left(\frac{e^2}{1 - \lambda^{-2}} \,\middle|\, e\right) \tag{6.16}$$

where K and Π are the complete elliptic integrals of the first and third kind. Together the product of Eqs. (6.15) and (6.16) into (6.9) give the reversal time for an ellipse. The mean reversal time for a needle is compared to different ellipses in Fig. 11. △

6.3. **Asymptotics of mean reversal time.** The integrand in Eq. (6.8) is the inverse of $\mathcal{P}(\theta) = c_1 w(\theta) \, \mathrm{e}^{\Phi(\theta)}$. The integral itself will thus typically be dominated by the minima of $\mathcal{P}$, which correspond to values of θ that the swimmer finds difficult to cross when trying to reverse. This could be because $\delta = 1 - \ell/L$ is small: this is the *narrow escape* problem discussed by Holcman & Schuss [37] (see Example 7). However, for a swimmer the long reversal time is usually due to a swimmer 'sticking' to the top or bottom wall for long times.
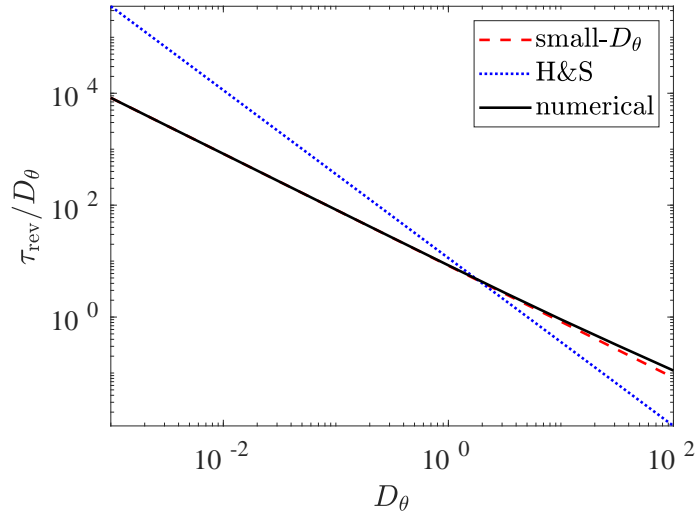
FIGURE 10. Mean reversal time for a needle as a function of D_θ, for $\lambda = .9$, $D_Y = 1$. The dashed line is (6.11), which is technically valid for small D_θ but applies over a wide range. The dotted line is from [37]. The solid line is from a finite-element simulation of the full PDE.
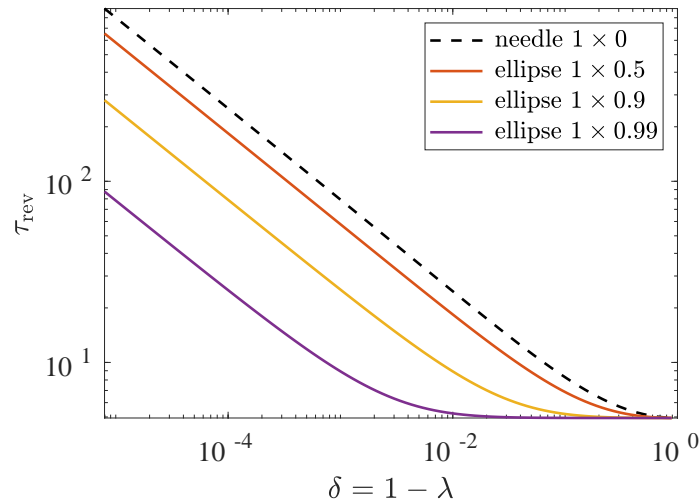

FIGURE 11. Mean reversal time τ_{rev} for a needle and different ellipses, as a function of gap size δ. An ellipse reverses more rapidly as it becomes more circular, since it spends less time aligning with the wall.

To approximate the integral in (6.8), we look for minima θ_* of $\mathcal{P}(\theta)$, where we can approximate

$$\mathcal{P}(\theta) = \mathcal{P}(\theta_*)\, e^{C_* \xi^2 + O(\xi^3)}, \qquad \xi = \theta - \theta_*. \tag{6.17}$$

This gives us the approximation

$$\tau_{\mathrm{rev}} \approx \frac{1}{4\mathcal{P}(\theta_*)} \int_{-\infty}^{\infty} e^{-C_* \xi^2}\, \mathrm{d}\vartheta = \frac{1}{4\mathcal{P}(\theta_*)} \sqrt{\frac{\pi}{C_*}}. \tag{6.18}$$

This should be multiplied by the number of minima with value $\mathcal{P}(\theta_*)$ in $0 \le \theta < \pi$, should there be more than one. We can easily obtain a more accurate, if messier, approximation by retaining higher-order terms in (6.17).

Example 8 (mean reversal time for a fast needle swimmer). An ideal example for the asymptotic approximation of τ_{rev} is the fast needle swimmer of Example 5. Figure 9b clearly shows strong peaks in $1/\mathcal{P}$ at $\theta_* = \pm\pi/2$ even for this modest value of U. Hence, we are justified in expanding around the minimum of (5.17) at $\theta_* = \pi/2$, which gives

$$\mathcal{P}(\theta_*) = \sqrt{\frac{\beta}{4\pi}}\, \alpha^{\beta/(1-\alpha)}, \qquad C_* = \beta/\alpha. \tag{6.19}$$

Recall that $\alpha = D_X/D_Y$ is the ratio of diffusivities, and β is a large Péclet number defined in Eq. (5.16). Inserting these in Eq. (6.18), we find

$$\tau_{\mathrm{rev}} \approx \frac{\pi}{2\beta}\, \alpha^{\frac{1}{2} - \frac{\beta}{1-\alpha}}, \tag{6.20}$$

or in the case $\alpha = 1$:

$$\tau_{\mathrm{rev}} \approx \frac{\pi}{2\beta}\, e^{\beta}, \qquad \alpha = 1. \tag{6.21}$$

This is exponential in the Péclet number β, so that the reversal time can become extremely long. Note also that the mean reversal time is independent of the channel width L in this limit. For the parameters in Fig. 9 ($\beta = 3.6$), the numerical mean reversal time is $\tau_{\mathrm{rev}} \approx 1.54 \times 10^3$, whereas the approximation (6.20) gives 1.38×10^3. The approximation is thus reasonably good even for a modest Péclet number β.   △

7. Effective diffusion along the channel

For the open channel configuration, as a microswimmer travels down the channel, it will occasionally reverse direction. For long times, we expect these reversals to lead to an effective diffusion process on large scales. One way to capture this limit exactly is to derive an effective diffusion equation using a homogenization approach [12, 67, 72, 85]. We proceed to do so for our microswimmer in a channel, and find the effective diffusivity in the same reduced limit as in Section 4 (small D_θ).

7.1. **Homogenized equation.** Rewrite the Fokker–Planck Eq. (3.3) as

$$\partial_t p + \partial_x(u\,p) + \partial_y(v\,p) = \partial_x^2(D_{xx}\,p) + 2\partial_x\partial_y(D_{xy}\,p) + \partial_y^2(D_{yy}\,p) + \partial_\theta^2(D_\theta\,p) \quad (7.1)$$

where $\boldsymbol{U} = (u, v)$. In this section we only assume that $\mathbb{D}$, D_θ, and $\boldsymbol{U}$ do not depend on x. (The derivation could easily be extended to allow x dependence.) Later (Section 7.2) we will specialize to the forms in Eq. (3.4), which are functions of θ only.

We will homogenize in the x direction only, since the swimmer is confined between walls in the y direction and the θ direction is periodic. We introduce a large scale x/η and long time t/η^2, where η is a small expansion parameter. After rescaling $t \to t/\eta^2$ and $x \to x/\eta$, Eq. (7.1) becomes

$$\mathcal{L}\,p = -\eta\,\partial_x(u\,p) + 2\eta\,\partial_x\partial_y(D_{xy}\,p) - \eta^2\partial_t p + \eta^2\,\partial_x^2(D_{xx}\,p) \qquad (7.2\text{a})$$

where we defined the linear operator

$$\mathcal{L}\,p := \partial_y(v\,p) - \partial_y^2(D_{yy}\,p) - \partial_\theta^2(D_\theta\,p). \qquad (7.2\text{b})$$

The no-flux boundary conditions for (7.2a) are

$$(v\,p - \partial_y(D_{yy}\,p) - \eta\,\partial_x(D_{xy}\,p)) + \zeta'_\pm(\theta)\,\partial_\theta(D_\theta\,p) = 0, \qquad y = \zeta_\pm(\theta). \qquad (7.2\text{c})$$

We expand the probability density p as a regular series in η:

$$p = p_0 + \eta\,p_1 + \eta^2\,p_2 + \dots. \qquad (7.3)$$

Define the cell integral of $f(\theta, y)$ as

$$\langle f \rangle := \int_{-\pi}^{\pi} \int_{\zeta_-(\theta)}^{\zeta_+(\theta)} f(\theta, y)\,\mathrm{d}y\,\mathrm{d}\theta. \qquad (7.4)$$

To ensure uniqueness at each order, we enforce the cell-integrated probability $\langle p \rangle = \langle p_0 \rangle$, so that $\langle p_i \rangle = 0$ for $i > 0$.

Now we collect powers of η in Eq. (7.2) with the expansion (7.3). At leading order in η we have from Eq. (7.2a)

$$\mathcal{L}\,p_0 = 0 \qquad (7.5\text{a})$$

with boundary conditions from Eq. (7.2c):

$$v\,p_0 - \partial_y(D_{yy}\,p_0) + \zeta'_\pm(\theta)\,\partial_\theta(D_\theta\,p_0) = 0, \qquad y = \zeta_\pm(\theta). \qquad (7.5\text{b})$$

The operator $\mathcal{L}$ only involves (θ, y), so we can solve Eq. (7.5) with

$$p_0 = \mathrm{P}(x, t)\,\rho(\theta, y), \qquad \mathcal{L}\rho = 0, \quad \langle \rho \rangle = 1, \qquad (7.6)$$

where $\rho(\theta, y)$ is the cell-normalized x-independent invariant density for (7.1), and so $\langle p_0 \rangle = \mathrm{P}(x, t)$.

At order η^1, Eq. (7.2a) gives

$$\mathcal{L}\,p_1 = -\partial_x(u\,p_0) + 2\partial_x\partial_y(D_{xy}\,p_0)$$
$$= (-u\,\rho + 2\partial_y(D_{xy}\,\rho))\,\partial_x\mathrm{P}. \tag{7.7}$$

We can solve this by letting

$$p_1 = \chi\,\partial_x\mathrm{P} \tag{7.8}$$

where $\chi(\theta, y)$ satisfies the *cell problem*

$$\mathcal{L}\,\chi = -u\,\rho + 2\partial_y(D_{xy}\,\rho); \tag{7.9a}$$
$$0 = v\,\chi - \partial_y(D_{yy}\,\chi) + \zeta'_{\pm}(\theta)\,\partial_\theta(D_\theta\,\chi) - D_{xy}\,\rho, \qquad y = \zeta_{\pm}(\theta), \tag{7.9b}$$

with $\langle\chi\rangle = 0$. The solvability condition for the cell problem (7.9) demands

$$\langle u\,\rho\rangle = \langle\partial_y(D_{xy}\,\rho)\rangle. \tag{7.10}$$

In our case, the left and right sides of (7.10) vanish separately after using the channel symmetry $\rho(\theta + \pi, y) = \rho(\theta, -y)$. On the left, we have $u(\theta) = U\cos\theta$, so $u(\theta + \pi) = -u(\theta)$ and the integral must vanish. On the right, we have $D_{xy}(\theta) = \frac{1}{2}(D_X - D_Y)\sin 2\theta$ from (3.4), so $D_{xy}(\theta + \pi) = D_{xy}(\theta)$ and $\partial_y\rho(\theta + \pi, y) = -(\partial_y\rho)(\theta, -y)$ and the integral again vanishes. There is thus no 'ratchet effect' to cause a net drift, since there is no breaking of the left-right symmetry of the channel. Having patterned walls as in Yariv and Schnitzer [122] would possibly cause such a drift.

At order η^2, Eq. (7.2) gives

$$\mathcal{L}\,p_2 = -\partial_x(u\,p_1) + 2\partial_x\partial_y(D_{xy}\,p_1) - \partial_t p_0 + \partial_x^2(D_{xx}\,p_0) \tag{7.11a}$$
$$0 = (v\,p_2 - \partial_y(D_{yy}\,p_2) - \partial_x(D_{xy}\,p_1)) + \zeta'_{\pm}(\theta)\,\partial_\theta(D_\theta\,p_2), \qquad y = \zeta_{\pm}(\theta). \tag{7.11b}$$

The solvability condition then yields the effective heat equation

$$\partial_t\mathrm{P} = D_{\mathrm{eff}}\,\partial_x^2\mathrm{P} \tag{7.12}$$

where the effective diffusivity in x is

$$D_{\mathrm{eff}} = \langle D_{xx}\,\rho\rangle - \langle u\,\chi\rangle + \langle\partial_y(D_{xy}\chi)\rangle. \tag{7.13}$$

The solvability condition (7.10) implies that χ only affects the effective diffusivity up to an additive multiple of ρ.

7.2. Reduced equation limit. We solve the cell problem (7.9) in the same small-D_θ limit as in Section 4. Anticipating that the effective diffusivity should diverge as $\varepsilon = D_\theta$ becomes smaller, we expand

$$\chi = \varepsilon^{-1}\,\chi_0 + \chi_1 + \varepsilon\,\chi_2 + \dots. \tag{7.14}$$

The leading-order ε^{-1} cell problem (7.9) is the the same as (4.3), with solution

$$\chi_0(\theta, y) = \mathrm{X}(\theta)\,\mathrm{e}^{\sigma(\theta)y}. \tag{7.15}$$

At next order ε^0 we have the PDE and boundary conditions

$$U \sin\theta \, \partial_y \chi_1 - D_{yy}(\theta) \, \partial_y^2 \chi_1 = \partial_\theta^2 \chi_0 - (U \cos\theta - 2\sigma D_{xy}) \, \mathcal{Q}(\theta) \, e^{\sigma(\theta)y}; \qquad (7.16a)$$

$$U \sin\theta \, \chi_1 - D_{yy}(\theta) \, \partial_y \chi_1 = -\zeta'_\pm(\theta) \, \partial_\theta \chi_0 + D_{xy} \, \mathcal{Q}(\theta) \, e^{\sigma(\theta)y}, \qquad y = \zeta_\pm(\theta), \quad (7.16b)$$

where we used the invariant density $\bar{p}_0 = \mathcal{Q}(\theta) \, e^{\sigma(\theta)y}$. Integrate (7.16a) from $y = \zeta_-$ to ζ_+ and use the boundary conditions (7.16b):

$$\partial_\theta(\nu X - w \, \partial_\theta X) = -\Xi \, \mathcal{P}, \qquad (7.17)$$

where $\mathcal{P} = w \mathcal{Q}$, and

$$\Xi(\theta) := U \cos\theta - \sigma D_{xy} = \frac{U \cos\theta}{\cos^2\theta + \alpha \sin^2\theta} \qquad (7.18)$$

with $\alpha = D_X/D_Y$ as in (5.17). We integrate Eq. (7.17) once:

$$\nu X - w \, \partial_\theta X = d - H(\theta), \qquad H(\theta) := \int_{-\pi}^{\theta} \Xi(\vartheta) \, \mathcal{P}(\vartheta) \, d\vartheta, \qquad (7.19)$$

with d a constant of integration. The solvability condition (7.10) ensures that $H(\theta)$ is a periodic function of θ. Next use the integrating factor $e^{\Phi(\theta)}$ from (5.4), with $\theta^L = -\pi$:

$$w \, e^{\Phi} \, \partial_\theta(e^{-\Phi} X) = H(\theta) - d. \qquad (7.20)$$

We integrate again and find

$$e^{-\Phi(\theta)} \, X(\theta) - X(-\pi) = \int_{-\pi}^{\theta} \frac{H(\vartheta)}{w(\vartheta) \, e^{\Phi(\vartheta)}} \, d\vartheta - c_1 d \, F(\theta) \qquad (7.21)$$

where we used $F(\theta)$ from Eq. (5.4). By rearranging and using Eq. (5.7), we find after introducing new constants

$$X(\theta) = \tilde{c}_1 \, e^{\Phi(\theta)} \left(\int_{-\pi}^{\theta} \frac{H(\vartheta)}{\widetilde{\mathcal{P}}(\vartheta)} \, d\vartheta - d_2 F(\theta) \right) + d_1 \mathcal{Q}(\theta) \qquad (7.22)$$

where we used $\widetilde{\mathcal{P}} = \tilde{c}_1 w \, e^{\Phi}$ as in Section 6.1. The constant d_1 is adjusted to satisfy $\langle \chi \rangle = 0$ and is immaterial to the effective diffusivity. The constant d_2 is used to enforce periodicity of X and can be eliminated to obtain

$$X(\theta) = \tilde{c}_1 \, e^{\Phi(\theta)} \left(\int_{-\pi}^{\theta} \frac{H(\vartheta)}{\widetilde{\mathcal{P}}(\vartheta)} \, d\vartheta - \frac{F(\theta)}{F(\pi)} \int_{-\pi}^{\pi} \frac{H(\vartheta)}{\widetilde{\mathcal{P}}(\vartheta)} \, d\vartheta \right) + d_1 \mathcal{Q}(\theta). \qquad (7.23)$$

In this reduced limit, the effective diffusivity Eq. (7.13) is

$$D_{\text{eff}} = \mathbb{E} D_{xx} + D_{\text{enh}}, \qquad D_{\text{enh}} := -\int_{-\pi}^{\pi} \Xi \, w X \, d\theta, \qquad (7.24)$$

to leading order in D_θ. The expected value $\mathbb{E}D_{xx}$ is taken over the invariant marginal density $\mathcal{P}(\theta)$, and D_{enh} is the 'enhanced' part of the diffusivity.

7.3. Bounding D_{eff} by τ_{rev} for a left-right symmetric swimmer.

Since the expressions are getting a bit complicated, for the sake of brevity we will focus on the left-right symmetric case for this section. In that case the term involving $F(\theta)$ vanishes in (7.23), and $\tilde{c}_1\, e^\Phi$ becomes $\mathcal{Q}$:

$$\mathrm{X}(\theta) = \mathcal{Q}(\theta) \int_{-\pi}^{\theta} \frac{H(\vartheta)}{\mathcal{P}(\vartheta)}\, \mathrm{d}\vartheta + d_1\mathcal{Q}(\theta). \tag{7.25}$$

After restoring in Eq. (7.25) the definition of H from Eq. (7.19), it can be shown that the enhanced diffusivity D_{enh} in Eq. (7.24) can be written as

$$D_{\text{enh}} = 4 \int_0^{\pi/2} \Xi(\theta)\, \mathcal{P}(\theta) \int_0^{\theta} \Xi(\theta')\, \mathcal{P}(\theta') \int_\theta^{\pi-\theta} \frac{\mathrm{d}\theta''}{\mathcal{P}(\theta'')}\, \mathrm{d}\theta'\, \mathrm{d}\theta. \tag{7.26}$$

To derive this we used the symmetries $\Xi(\theta + \pi) = \Xi(\pi - \theta) = -\Xi(\theta)$, $\mathcal{P}(\theta + \pi) = \mathcal{P}(\pi - \theta) = \mathcal{P}(\theta)$, the latter holding for a left-right-symmetric swimmer. Rearranging the innermost integral in (7.27) gives us

$$D_{\text{enh}} = \tfrac{1}{2}\tau_{\text{rev}}(\mathbb{E}|\Xi|)^2 - 8 \int_0^{\pi/2} \Xi(\theta)\, \mathcal{P}(\theta) \int_0^{\theta} \Xi(\theta')\, \mathcal{P}(\theta)' \int_0^{\theta} \frac{\mathrm{d}\theta''}{\mathcal{P}(\theta'')}\, \mathrm{d}\theta'\, \mathrm{d}\theta, \tag{7.27}$$

where the mean reversal time τ_{rev} was defined in Eq. (6.8). The expected value in (7.27) is taken over the invariant marginal density $\mathcal{P}(\theta)$, as in Eq. (7.24).

Since $\Xi(\theta)$ defined by Eq. (7.18) is non-negative in $[0, \pi/2]$, Eq. (7.27) immediately gives us the bound

$$D_{\text{enh}} \leq \tfrac{1}{2}\tau_{\text{rev}}(\mathbb{E}|\Xi|)^2 \leq \tfrac{1}{2}\tau_{\text{rev}}\, \max_\theta \Xi^2(\theta), \tag{7.28a}$$

with

$$\max_{0 \leq \theta \leq \pi/2} \Xi(\theta) = \begin{cases} U, & \alpha \geq 1/2; \\ U/\sqrt{4\alpha(1-\alpha)}, & \alpha < 1/2. \end{cases} \tag{7.28b}$$

This useful bound allows us to estimate D_{enh} from τ_{rev}, which is simpler to compute (Eq. (6.8)). The estimate tends to improve the longer the swimmer spends aligned with the walls (Fig. 12).

8. Discussion

We used both theory and numerics to analyze the dynamics of finite-sized swimmers in a channel. The shape of swimmers is embedded in their configuration space, which is defined even for nonsmooth swimmers via their convex hull. Shape enters solely in the boundary conditions to the Fokker–Planck equation. We then derived a reduced equation in the small D_θ limit for both open and closed channels, from which
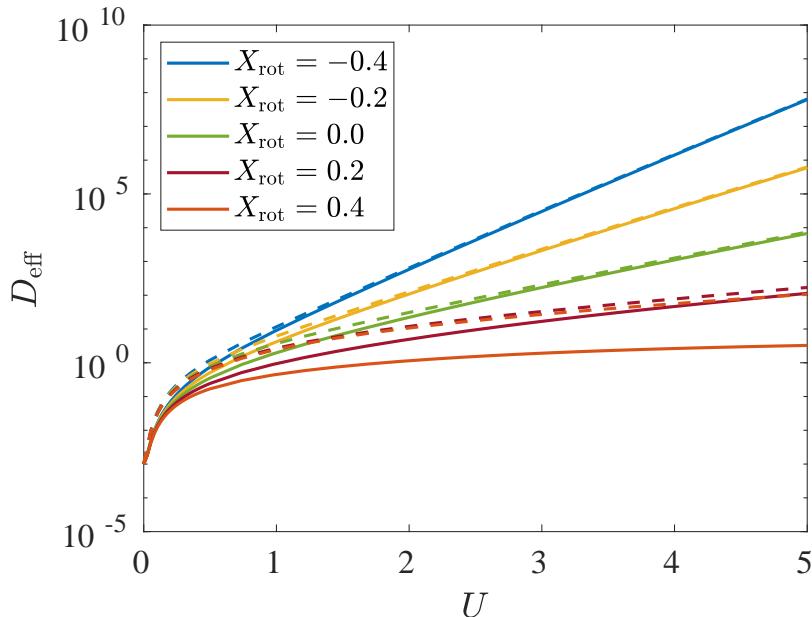
FIGURE 12. Effective diffusivity from Eq. (7.24) for an ellipse with $a = 1$, $b = 1/2$, $D_X = D_Y = 0.1$, $D_\theta = 0.01$, in a channel of width $L = 1.2$. The dashed lines are the bound $\frac{1}{2}U^2\tau_{\rm rev}$ from (7.28), with $\alpha = 1$ and $\tau_{\rm rev}$ given by Eq. (6.8). The decrease in exponential rate as the center of rotation $X_{\rm rot}$ is moved forward is similar to the asymptotic form of $\tau_{\rm rev}$ for a needle, Eq. (6.21), with β given by (5.16).

we computed the invariant density. For open channel geometry, we calculated the mean reversal time. We used homogenization techniques and solved the cell problem to find the effective diffusivity. The shape of a swimmer is encoded in the rotational drift term μ in the reduced equation (4.15), and appears explicitly in the integral solution for the invariant density, mean reversal time, and effective diffusivity. The integral of μ vanishes for a left-right symmetric swimmer, and many of our expressions then greatly simplify. In particular the mean angular drift vanishes for such a symmetric swimmer.

A particular novelty in our work is to explicitly allow the position of the center of rotation, $X_{\rm rot}$, to vary. The sign of $X_{\rm rot}$ affects the configuration space, as shown in Fig. 4, and changes a swimmers' tendency to align with walls. When a swimmer's center of rotation is behind its geometrical center, it tends to align with a wall; in the opposite case, it tends to stay perpendicular to the wall even for a needle or circular swimmer (Examples 5 and 6).

In our work we focused on two-dimensional swimmers for simplicity and ease of presentation. However, generalizing the formalism to three-dimensional axisymmetric swimmers is straightforward [77]. In that case, the wall distance function y_* is essentially the same as in 2D, and all that changes is that the ∂_θ^2 operator must be replaced by the 3D surface Laplacian. The dynamics for 3D axisymmetric swimmers will thus be similar to 2D left-right symmetric swimmers, with some quantitative changes. In particular, following almost the same calculations, we found the invariant density is given by a formula similar to Eq. (5.21), and when applied to spherical swimmers with $X_{\mathrm{rot}} = 0$ it agrees with the results in [23, 29]. A Fully 3D swimmer that is not axisymmetric will require considerably more work to implement: the configuration space has an extra dimension due to the extra degrees of freedom. Of course, this will potentially also make the dynamics richer, and will allow for interesting effects such as chirality.

Another challenging direction is to add hydrodynamic interactions with boundaries, in a manner similar to the work mentioned in the introduction. This is in principle straightforward, though the equations will be harder to solve. Here, we left out these interactions in order to emphasize steric effects and keep the equations simple, permitting analytic solutions. It is also possible to include variable swimmer shapes, which would allow the inclusion of flagella, by letting the configuration space itself be time-dependent.

Acknowledgments

References

1. B. Ai, Q. Chen, Y. He, F. Li, and W. Zheng, *Rectification and diffusion of self-propelled particles in a two-dimensional corrugated channel*, Phys. Rev. E **88** (2013), 062129.
2. R. Alonso-Matilla, B. Ezhilan, and D. Saintillan, *Microfluidic rheology of active particle suspensions: Kinetic theory*, Biomicrofluidics **10** (2016), 043505.
3. R. Alonso-Matilla and D. Saintillan, *Interfacial instabilities in active viscous films*, J. Non-Newtonian Fluid Mech. **259** (2019), 57–64.
4. R. N. Bearon, A. L. Hazel, and G. J. Thorn, *The spatial distribution of gyrotactic swimming micro-organisms in laminar flow fields*, J. Fluid Mech. **680** (2011), 602–635.
5. C. Bechinger, R. Di Leonardo, H. Löwen, C. Reichhardt, G. Volpe, and G. Volpe, *Active particles in complex and crowded environments*, Rev. Mod. Phys. **88** (2016), 045006.

6. A. P. Berke, L. Turner, H. C. Berg, and E. Lauga, *Hydrodynamic attraction of swimming microorganisms by surfaces*, Phys. Rev. Lett. **101** (2008), 038102.

7. S. Bianchi, F. Saglimbeni, and R. Di LEonardo, *Holographic imaging reveals the mechanism of wall entrapment in swimming bacteria*, Phys. Rev. X **7** (2017), 011010.

8. A. Bricard, J.-B. Caussin, D. Dasand C. Savoie, V. Chikkadi, K. Shitara, O. Chepizhko, F. Peruani, D. Saintillan, and D. Bartolo, *Emergent vortices in populations of confined colloidal rollers*, Nat. Commun. **6** (2015), 7470.

9. L. Caprini and U. Marconi, *Active particles under confinement and effective force generation among surfaces*, Soft Matter **14** (2018), 9044–9054.

10. M. E. Cates and J. Tailleur, *When are active Brownian particles and run-and-tumble particles equivalent? Consequences for motility-induced phase separation*, Europhys. Lett. **101** (2013), 20010.

11. Y. Chen, Z. Wang, K. Chu, H.Chen, Y. Sheng, and H. Tsao, *Hydrodynamic interaction induced breakdown of the state properties of active fluids*, Soft Matter **14** (2018), 5319–5326.

12. S. Childress and A. M. Soward, *Scalar transport and alpha-effect for a family of cats-eye flows*, J. Fluid Mech. **205** (1989), 99–133.

13. S. Chilukuri, C. H. Collins, and P. T. Underhill, *Impact of external flow on the dynamics of swimming microorganisms near surfaces*, J. Phys.: Condens. Matter **26** (2014), 115101.

14. M. Contino, E. Lushi, I. Tuval, V. Kantsler, and M. Polin, *Microalgae scatter off solid surfaces by hydrodynamic and contact forces*, Phys. Rev. Lett. **115** (2015), no. 25, 258102.

15. A. Costanzo, R. Di Leonardo, G. Ruocco, and L. Angelani, *Transport of self-propelling bacteria in micro-channel flow*, J. Phys.: Condens. Matter **24** (2012), 065101.

16. D. G. Crowdy and Y. Or, *Two-dimensional point singularity model of a low-Reynolds-number swimmer near a wall*, Phys. Rev. E **81** (2010), 036313.

17. D. G. Crowdy and O. Samson, *Hydrodynamic bound states of a low-Reynolds-number swimmer near a gap in a wall*, J. Fluid Mech. **667** (2011), 309–335.

18. A. Daddi-Moussa-Ider, M. Lisicki, C. Hoell, and H. Löwen, *Swimming trajectories of a three-sphere microswimmer near a wall*, J. Chem. Phys. **148** (2018), 134904.

19. P. Denissenko, V. Kanstler, D. J. Smith, and J. Kirkman-Brown, *Human spermatozoa migration in micro channels reveals boundary-following navigation*, Proc. Natl. Acad. Sci. USA **109** (2012), 8007–8010.

20. W. R. DiLuzio, L. Turner, M. Mayer, P. Garstecki, D. B. Weibel, H. C. Berg, and G.e M. Whitesides The, *Escherichia coli swim on the right-hand side*, Nature **435** (2005), 1271–1274.

21. K. Drescher, J. Dunkel, L. H. Cisneros, S. Ganguly, and R. E. Goldstein, *Fluid dynamics and noise in bacterial cell-cell and cell-surface scattering*, Proc. Natl. Acad. Sci. USA **108** (2011), 10940–10945.

22. J. Elgeti and G. Gompper, *Self-propelled rods near surfaces*, Europhys. Lett. **85** (2009), 38002.

23. _____, *Wall accumulation of self-propelled spheres*, Europhys. Lett. **101** (2013), 48003.

24. _____, *Run-and-tumble dynamics of self-propelled particles in confinement*, Europhys. Lett. **109** (2015), 58003.

25. _____, *Microswimmers near surfaces*, Eur. Phys. J. Spec. Top. **225** (2016), 2333–2352.

26. A. A. Evans and E. Lauga, *Propulsion by passive filaments and active flagella near boundaries*, Phys. Rev. E **82** (2010), 041915.

27. B. Ezhilan, R. Alonso-Matilla, and D. Saintillan, *On the distribution and swim pressure of run-and-tumble particles in confinement*, J. Fluid Mech. **781** (2015), R4.

28. B. Ezhilan, A. A. Pahlavan, and D. Saintillan, *Chaotic dynamics and oxygen transport in thin films of aerotactic bacteria*, Phys. Fluids **24** (2012), 091701.

29. B. Ezhilan and D. Saintillan, *Transport of a dilute active suspension in pressure-driven channel flow*, J. Fluid Mech. **777** (2015), 482–522.

30. L. J. Fauci and A. McDonald, *Sperm motility in the presence of boundaries*, Bull. Math. Biol. **57** (1995), 679–699.

31. P. D. Frymier, R. M. Ford, H. C. Berg, and P. T. Cummings, *Three-dimensional tracking of motile bacteria near a solid planar surface*, Proc. Natl. Acad. Sci. USA **92** (1995), 6195–6199.

32. D. S. Grebenkov, *Universal formula for the mean first passage time in planar domains*, Phys. Rev. Lett. **117** (2016), 260201.

33. J. Happel and H. Brenner, *Low Reynolds number hydrodynamics*, Martinus Nijhoff (Kluwer), The Hague, Netherlands, 1983.

34. J. P. Hernandez-Ortiz, C. G. Stoltz, and M. D. Graham, *Transport and collective dynamics in suspensions of confined swimming particles*, Phys. Rev. Lett. **95** (2005), 204501.

35. J. P. Hernandez-Ortiz, P. T. Underhill, and M. D. Graham, *Dynamics of confined suspensions of swimming particles*, J. Phys.: Condens. Matter **21** (2009), 204107.

36. J. Hill, O. Kalkanci, J. L. McMurry, and H. Koser, *Hydrodynamic surface interactions enablei Escherichia coli to seek efficient routes to swim upstream*, Phys. Rev. Lett. **98** (2007), 068101.

37. D. Holcman and Z. Schuss, *The narrow escape problem*, SIAM Review **56** (2014), no. 2, 213–257.

38. A. Kaiser, H. H. Wensink, and H. Löwen, *How to capture active particles*, Phys. Rev. Lett. **108** (2012), 268307.

39. V. Kantsler, J. Dunkel, M. Polin, and R. E. Goldstein, *Ciliary contact interactions dominate surface scattering of swimming eukaryotes*, Proc. Natl. Acad. Sci. USA **110** (2013), no. 4, 1187–1192.

40. D. F. Katz, *Propulsion of microorganisms near solid boundaries*, J. Fluid Mech. **64** (1974), 33–49.

41. D. F. Katz and J. R. Blake, *flagellar motions near walls*, Swimming and Flying in Nature **1** (1975), 173–184.

42. D. F. Katz, J. R. Blake, and S. L. Paverifontana, *On the movement of slender bodies near plane boundaries at low Reynolds number*, J. Fluid Mech. **72** (1975), 529–540.

43. U. Kaynan and E. Yariv, *Stokes resistance of a cylinder near a slippery wall*, Phys. Rev. Fluids **2** (2017), 104103.

44. M. Y. Kim, K. Drescher, O. S. Park, B. Bassler, and H. A. Stone, *Filaments in curved streamlines: rapid formation of Staphylococcus aureus biofilm streamers*, New J. Phys. **16** (2014), 065024.

45. N. Koumakis, C. Maggi, and R. Di Leonardo, *Directed transport of active particles over asymmetric energy barriers*, Soft Matter **10** (2014), 5695–5701.

46. P. J. Krochak, J. A. Olson, and D.M. Martinez, *Near-wall estimates of the concentration and orientation distribution of a semi-dilute rigid fibre suspension in Poiseuille flow*, J. Fluid Mech. **653** (2010), 431–462.

47. V. Kurella, J. C. Tzou, D. Coombs, and M. J. Ward, *Asymptotic analysis of first passage time problems inspired by ecology*, Bull. Math. Biol. **77** (2015), no. 1, 83–125.

48. C. Kurzthaler and T. Franosch, *Intermediate scattering function of an anisotropic Brownian circle swimmer*, Soft Matter **13** (2017), 6396–6406.

49. C. Kurzthaler, S. Leitmann, and T. Franosch, *Intermediate scattering function of an anisotropic active Brownian particle*, Sci. Rep. **6** (2016), 36702.

50. G. Lambert, D. Liao, and R. H. Austin, *Collective escape of chemotactic swimmers through microscopic ratchets*, Phys. Rev. Lett. **104** (2010), 168102.

51. E. Lauga, *Swimming in circles: Motion of bacteria near solid boundaries*, Biophys. J. **90** (2006), 400–412.

52. E. Lauga and T. R. Powers, *The hydrodynamics of swimming microorganisms*, Rep. Prog. Phys. **72** (2009), 096601.

53. C. F. Lee, *Active particles under confinement: aggregation at the wall and gradient formation inside a channel*, New J. Phys. **15** (2013), 055007.

54. M. Lee, K. Szuttor, and C. Holm, *A computational model for bacterial run-and-tumble motion*, J. Chem. Phys. **17** (2019), 174111.

55. A. Lefauve and D. Saintillan, *Globally aligned states and hydrodynamic traffic jams in confined suspensions of active asymmetric particles*, Phys. Rev. E **89** (2014), 021002.

56. G. Li, J. Bensson, L. Nisimova, D. Munger, P. Mahautmr, J. X. Tang, M. R. Maxey, and Y.V. Brun, *Accumulation of swimming bacteria near a solid surface*, Phys. Rev. E **84** (2011), 041932.

57. G. Li, L. Tam, and J. Tanf, *Amplified effect of Brownian motion in bacterial near-surface swimming*, Proc. Natl. Acad. Sci. USA **105** (2008), 18355–18359.

58. G. Li and J. X. Tang, *Accumulation of microswimmers near a surface mediated by collision and rotational Brownian motion*, Phys. Rev. Lett. **103** (2009), 078101.

59. G.-J. Li and A. M. Ardekani, *Hydrodynamic interaction of microswimmers near a wall*, Phys. Rev. E **90** (2014), 013010.

60. D. Lopez and E. Lauga, *Dynamics of swimming bacteria at complex interfaces*, Phys. Fluids **26** (2014), 071902.

61. E. Lushi, *Stability and dynamics of anisotropically-tumbling chemotactic swimmers*, Phys. Rev. E **94** (2016), 022414.

62. E. Lushi, R. E. Goldstein, and M. J. Shelley, *Collective chemotactic dynamics in the presence of self-generated fluid flows*, Phys. Rev. E **86** (2012), 040902.

63. ———, *Nonlinear concentration patterns and bands in autochemotactic suspensions*, Phys. Rev. E **98** (2018), 052411.

64. E. Lushi, V. Kantsler, and R. E. Goldstein, *Scattering of biflagellate microswimmers from surfaces*, Phys. Rev. E **96** (2017), no. 2, 023102.

65. E. Lushi and P. M. Vlahovska, *Periodic and chaotic orbits of plane-confined micro-rotors in creeping flows*, J. Nonlinear Sci. Appl. **25** (2015), 1111–1123.

66. E. Lushi, H. Wioland, and R. E. Goldstein, *Fluid flows created by swimming bacteria drive self-organization in confined suspensions*, Proc. Natl. Acad. Sci. USA **111** (2014), no. 27, 9733–9738.

67. A. J. Majda and P. R. Kramer, *Simplified models for turbulent diffusion: Theory, numerical modelling and physical phenomena*, Physics Reports **314** (1999), no. 4-5, 237–574.

68. M. C. Marchetti, J. F. Joanny, S. Ramaswamy, T. B. Liverpool, J. Prost, M. Rao, and R. A. Simha, *Hydrodynamics of soft active matter*, Rev. Mod. Phys. **85** (2013), 1143–1189.

69. F. Marcotte, C. R. Doering, J.-L Thiffeault, and W. R. Young, *Optimal heat transfer and optimal exit times*, SIAM J. Appl. Math. **78** (2018), no. 1, 591–608.

70. K. Martens, L. Angelani, R. Di Leonardo, and L. Bocquet, *Probability distributions for the run-and-tumble bacterial dynamics: An analogy to the lorentz model*, Europhys. Lett. **35** (2012), 1–6.

71. A. J. T. M. Mathijssen, A. Doostmohammadi, J. M. Yeomans, and T. N. Shendruk, *Hotspots of boundary accumulation: Dynamics and statistics of microswimmers in flowing films*, J. Roy. Soc. Interface **13** (2016), 20150936.

72. P. McCarty and W. Horsthemke, *Effective diffusion for steady two-dimensional flow*, Phys. Rev. A **37** (1988), no. 6, 2112–2117.

73. M. Mirzakhanloo and M.-R. Alam, *Flow characteristics of Chlamydomonas result in purely hydrodynamic scattering*, Phys. Rev. E **98** (2018), no. 1, 012603.

74. M. Molaei, M. Barry, R. Stocker, and J. Sheng, *Failed escape: Solid surfaces prevent tumbling of Escherichia coli*, Phys. Rev. Lett. **113** (2014), 068103.

75. R. W. Nash, R. Adhikari, J. Tailleur, and M. E. Cates, *Run-and-tumble particles with hydrodynamics: sedimentation, trapping, and upstream swimming*, Phys. Rev. Lett. **104** (2010), 258101.

76. N. Nikola, A. P. Solon, Y. Kafri, M. Kardar, J. Tailleur, and R. Voituriez, *Active particles with soft and curved walls: Equation of state, ratchets, and instabilities*, Phys. Rev. Lett. **117** (2016), 098001.

77. J. M. Nitsche and H. Brenner, *On the formulation of boundary conditions for rigid non spherical Brownian particles near solid walls: Applications to orientation-specific reactions with immobilized enzymes*, J. Colloid Interface Sci. **138** (1990), 21–41.

78. K. Obuse and J.-L. Thiffeault, *A low-Reynolds-number treadmilling swimmer near a semi-infinite wall*, IMA Volume on Natural Locomotion in Fluids and on Surfaces: Swimming, Flying, and Sliding (S. Childress, A. Hosoi, W. W. Schultz, and J. Wang, eds.), The IMA Volumes in Mathematics and its Applications, Springer, New York, 2012, pp. 197–206.

79. G. A. Pavliotis, *Stochastic processes and applications*, Springer, Berlin, 2014.

80. N. Razin, R. Voituriez, J. Elgeti, and N. S. Gov, *Generalized Archimedes' principle in active fluids*, Phys. Rev. E **96** (2017), 032606.

81. G. S. Redner, M. F. Hagan, and A. Baskaran, *Structure and dynamics of a phase-separating active colloidal fluid*, Phys. Rev. Lett. **110** (2013), 055701.

82. S. Redner, *A guide to first-passage processes*, Cambridge University Press, Cambridge, U.K., 2001.

83. L. Rothschild, *Non-random distribution of bull spermatozoa in a drop of sperm suspension*, Nature **198** (1963), 1221–1222.

84. R. Rusconi, S. Lecuyer, L. Guglielmini, and H. A. Stone, *Laminar flow around corners triggers the formation of biofilm streamers*, J. Roy. Soc. Interface **7** (2010), 1293–1299.

85. F. Sagues and W. Horsthemke, *Diffusive transport in spatially periodic hydrodynamic flows*, Phys. Rev. A **34** (1986), no. 5, 4136–4143.

86. D. Saintillan, *The dilute rheology of swimming suspensions: A simple kinetic model*, Exp. Mech. **50** (2010), 12751281.

87. D. Saintillan, E. S. G. Shaqfeh, and E. Darve, *Effect of flexibility on the shear-induced migration of short-chain polymers in parabolic channel flow*, J. Fluid Mech. **557** (2006), 297–306.

88. _____, *The growth of concentration fluctuations in dilute dispersions of orientable and deformable particles under sedimentation*, J. Fluid Mech. **553** (2006), 347–388.

89. D. Saintillan and M. J. Shelley, *Orientational order and instabilities in suspensions of self-locomoting rods*, Phys. Rev. Lett. **99** (2007), 058102.

90. _____, *Instabilities and pattern formation in active particle suspensions: Kinetic theory and continuum simulations*, Phys. Rev. Lett. **100** (2008), 178103.

91. _____, *Emergence of coherent structures and large-scale flows in motile suspensions*, J. Roy. Soc. Interface **9** (2011), 571–585.

92. _____, *Active suspensions and their nonlinear models*, C. R. Phys. **14** (2013), 497–517.

93. K. Schaar, A. Zöttl, and H. Stark, *Detention times of microswimmers close to surfaces: Influence of hydrodynamic interactions and noise*, Phys. Rev. Lett. **115** (2015), no. 3, 038101.

94. N. Sepúlveda and R. Soto, *Wetting transitions displayed by persistent active particles*, Phys. Rev. Lett. **119** (2017), 078001.

95. _____, *Universality of active wetting transitions*, Phys. Rev. E **98** (2018), 052141.

96. H. Shum, E. Gaffney, and D. Smith, *Modelling bacterial behaviour close to a no-slip plane boundary: The influence of bacterial geometry*, Proc. Royal Soc. A **466** (2010), 1725–1748.

97. O. Sipos, K. Nagy, R. Di Leonardo, and P. Galajda, *Hydrodynamic trapping of swimming bacteria by convex walls*, Phys. Rev. Lett. **114** (2015), 258104.

98. A. P. Solon, Y. Fily, A. Baskaran, M. E. Cates, Y. Kafri, M. Kardar, and J. Tailleur, *Pressure is not a state function for generic active fluids*, Nat. Phys. **11** (2015), 673678.

99. S. E. Spagnolie and E. Lauga, *Hydrodynamics of self-propulsion near boundaries: predictions and accuracy of far-field approximations*, J. Fluid Mech. **700** (2012), 105–147.

100. S. E. Spagnolie, G. R. Moreno-Flores, D. Bartolo, and E. Lauga, *Geometric capture and escape of a microswimmer colliding with an obstacle*, Soft Matter **11** (2015), 3396–3411.

101. T. Speck, *Collective forces in scalar active matter*, Soft Matter **16** (2020), 2652–2663.

102. J. Stenhammar, D. Marenduzzo, R.J. Allen, and M. E. Cates, *Phase behaviour of active Brownian particles: The role of dimensionality*, Soft Matter **10** (2014), 1489–1499.

103. J. W. Swan and J. F. Brady, *Simulation of hydrodynamically interacting particles near a no-slip boundary*, Phys. Fluids **19** (2007), 113306.
104. J. Tailleur and M. E. Cates, *Sedimentation, trapping, and rectification of dilute bacteria*, Europhys. Lett. **86** (2009), 60002.
105. D. Takagi, J. Palacci, A. Braunschweig, M. Shelley, and J. Zhang, *Hydrodynamic capture of microswimmers into sphere-bound orbits*, Soft Matter **10** (2014), 1784–1789.
106. S. C. Takatori, W. Yan, and J. F. Brady, *Swim pressure: Stress generation in active matter*, Phys. Rev. Lett. **113** (2014), 028103.
107. B. ten Hagen, R. Wittkowski, and H. Löwen, *Brownian dynamics of a self-propelled particle in shear flow*, Phys. Rev. E **84** (2011), 031105.
108. B. ten Hagen, R. Wittkowski, D. Takagi, F. Kümmel, C. Bechinger, and H. Löwen, *Can the self-propulsion of anisotropic microswimmers be described by using forces and torques*, J. Phys.: Condens. Matter **27** (2015), 194110.
109. M. Theers, E. Westphal, K. Qi, R. G. Winkler, and G. Gompper, *Clustering of microswimmers: interplay of shape and hydrodynamics*, Soft Matter **14** (2018), 8590–8603.
110. M. Theillard, R. A. Matilla, and D. Saintillan, *Geometric control of active collective motion*, Soft Matter **13** (2017), 363–375.
111. W. Tian, Y. Gu, Y. Guo, and K. Chen, *Anomalous boundary deformation induced by enclosed active particles*, Chin. Phys. B **26** (2017), 100502.
112. S. van Teeffelen and H. Löwen, *Dynamics of a Brownian circle swimmer*, Phys. Rev. E **78** (2008), 020101.
113. G. Volpe, I. Buttinoni, D. Vogt, H. J. Kümmerer, and C. Bechinger, *Microswimmers in patterned environments*, Soft Matter **7** (2011), 8810–8815.
114. G. Volpe, S. Gigan, and G. Volpe, *Simulation of the active Brownian motion of a microswimmer*, Am. J. Phys. **82** (2014), no. 7, 659–664.
115. C. Wagner, M. Hagan, and A. Baskaran, *Response of active Brownian particles to boundary driving*, Phys. Rev. E **100** (2019), 042610.
116. C. Wagner, M. F. Hagan, and A. Baskaran, *Steady-state distributions of ideal active Brownian particles under confinement and forcing*, J. Stat. Mech.: Theory Exp. (2017), 043203.
117. M. J. Ward and J. B. Keller, *Strong localized perturbations of eigenvalue problems*, SIAM J. Appl. Math. **53** (1993), no. 3, 770–798.
118. H. H. Wensink and H. Löwen, *Aggregation of self-propelled colloidal rods near confining walls*, Phys. Rev. E **78** (2008), 031409.
119. H. Wioland, E. Lushi, and R. E. Goldstein, *Directed collective motion of bacteria under channel confinement*, New J. Phys. **18** (2016), 081001.
120. D. M. Woolley, *Motility of spermatozoa at surfaces*, Reproduction **126** (2003), 259–270.

121. W. Yan and J. F. Brady, *The force on a boundary in active matter*, J. Fluid Mech. **785** (2015), R1.

122. E. Yariv and O. Schnitzer, *Ratcheting of Brownian swimmers in periodically corrugated channels: A reduced Fokker–Planck approach*, Phys. Rev. E **90** (2014), 032115.

123. K. Yeo, E. Lushi, and P. M. Vlahovska, *Collective dynamics in a binary mixture of hydrodynamically coupled micro-rotors*, Phys. Rev. Lett. **114** (2015), 188301.

124. R. Zargar, A. Najafi, and M. Miri, *Three-sphere low-Reynolds-number swimmer near a wall*, Phys. Rev. E **80** (2009), 026308.

125. A. Zöttl and H. Stark, *Emergent behavior in active colloids*, J. Phys.: Condens. Matter **28** (2016), 253001.

Appendix A. Derivation of the mean reversal time

In this Appendix we show how to from the reversal time formula Eq. (6.6) to the more explicit form (6.7) by eliminating the constant $\mathcal{C}$. First note that the numerator of Eq. (6.5) is

$$\int_{-\pi}^{\pi} \frac{\widetilde{G}(\vartheta)}{\widetilde{\mathcal{P}}(\vartheta)} \, \mathrm{d}\vartheta = \int_{-\pi}^{0} \frac{\widetilde{G}(\vartheta)}{\widetilde{\mathcal{P}}(\vartheta)} \, \mathrm{d}\vartheta + \int_{-\pi}^{0} \frac{\widetilde{G}(\vartheta + \pi)}{\widetilde{\mathcal{P}}(\vartheta + \pi)} \, \mathrm{d}\vartheta. \tag{A.1}$$

We wish to relate $\widetilde{\mathcal{P}}(\theta + \pi)$ to $\widetilde{\mathcal{P}}(\theta) = \tilde{c}_1 \, w(\theta) \, \mathrm{e}^{\Phi(\theta)}$. We have $w(\theta + \pi) = w(\theta)$. The change in Φ over a period is, from Eq. (5.4),

$$\Phi(\theta + \pi) - \Phi(\theta) = \int_0^{\pi} \mu(\vartheta) \, \mathrm{d}\vartheta = \pi\bar{\mu}, \tag{A.2}$$

since $\mu(\theta)$ is π-periodic. Here $\bar{\mu}$ is the period-averaged $\mu(\theta)$ from Eq. (5.11); $\Phi(\theta)$ is only π-periodic when $\bar{\mu} = 0$, or equivalently $c_2 = 0$. It follows from Eq. (A.2) that Φ must have the form

$$\Phi(\theta) = \bar{\mu}\,\theta + \tilde{\Phi}(\theta), \tag{A.3}$$

where $\tilde{\Phi}(\theta)$ is π-periodic. We conclude from $\widetilde{\mathcal{P}}(\theta) = \tilde{c}_1 \, w(\theta) \, \mathrm{e}^{\Phi(\theta)}$ that $\widetilde{\mathcal{P}}(\theta + \pi) = \mathrm{e}^{\pi\bar{\mu}} \, \widetilde{\mathcal{P}}(\theta)$. Similarly, for $-\pi \le \theta \le 0$,

$$\begin{aligned}
\widetilde{G}(\theta + \pi) &= \int_{-\pi}^{\theta + \pi} \widetilde{\mathcal{P}}(\vartheta) \, \mathrm{d}\vartheta \\
&= \int_{-\pi}^{0} \widetilde{\mathcal{P}}(\vartheta) \, \mathrm{d}\vartheta + \int_{0}^{\theta + \pi} \widetilde{\mathcal{P}}(\vartheta) \, \mathrm{d}\vartheta \\
&= \widetilde{G}(0) + \mathrm{e}^{\pi\bar{\mu}} \, \widetilde{G}(\theta).
\end{aligned} \tag{A.4}$$

Returning to Eq. (A.1), we obtain

$$\int_{-\pi}^{\pi} \frac{\widetilde{G}(\vartheta)}{\widetilde{\mathcal{P}}(\vartheta)}\, \mathrm{d}\vartheta = \int_{-\pi}^{0} \frac{\widetilde{G}(\vartheta)}{\widetilde{\mathcal{P}}(\vartheta)}\, \mathrm{d}\vartheta + \int_{-\pi}^{0} \frac{\widetilde{G}(0) + \mathrm{e}^{\pi\bar{\mu}}\, \widetilde{G}(\theta)}{\mathrm{e}^{\pi\bar{\mu}}\, \widetilde{\mathcal{P}}(\vartheta)}\, \mathrm{d}\vartheta$$

$$= 2 \int_{-\pi}^{0} \frac{\widetilde{G}(\vartheta)}{\widetilde{\mathcal{P}}(\vartheta)}\, \mathrm{d}\vartheta + \widetilde{G}(0)\, \mathrm{e}^{-\pi\bar{\mu}} \int_{-\pi}^{0} \frac{\mathrm{d}\vartheta}{\widetilde{\mathcal{P}}(\vartheta)}. \tag{A.5}$$

The denominator of $\mathcal{C}$ in (6.5) is

$$\int_{-\pi}^{\pi} \frac{\mathrm{d}\vartheta}{\widetilde{\mathcal{P}}(\vartheta)} = \int_{-\pi}^{0} \frac{\mathrm{d}\vartheta}{\widetilde{\mathcal{P}}(\vartheta)} + \int_{-\pi}^{0} \frac{\mathrm{d}\vartheta}{\widetilde{\mathcal{P}}(\vartheta + \pi)} = (1 + \mathrm{e}^{-\pi\bar{\mu}}) \int_{-\pi}^{0} \frac{\mathrm{d}\vartheta}{\widetilde{\mathcal{P}}(\vartheta)}. \tag{A.6}$$

Together (A.5) and (A.6) give

$$\mathcal{C} \int_{-\pi}^{0} \frac{\mathrm{d}\vartheta}{\widetilde{\mathcal{P}}(\vartheta)} = \frac{1}{1 + \mathrm{e}^{-\pi\bar{\mu}}} \left(2 \int_{-\pi}^{0} \frac{\widetilde{G}(\vartheta)}{\widetilde{\mathcal{P}}(\vartheta)}\, \mathrm{d}\vartheta + \widetilde{G}(0)\, \mathrm{e}^{-\pi\bar{\mu}} \int_{-\pi}^{0} \frac{\mathrm{d}\vartheta}{\widetilde{\mathcal{P}}(\vartheta)} \right). \tag{A.7}$$

We use this in the reversal time (6.6):

$$\tau_{\mathrm{rev}} = \mathcal{C} \int_{-\pi}^{0} \frac{\mathrm{d}\vartheta}{\widetilde{\mathcal{P}}(\vartheta)} - \int_{-\pi}^{0} \frac{\widetilde{G}(\vartheta)}{\widetilde{\mathcal{P}}(\vartheta)}\, \mathrm{d}\vartheta$$

$$= \frac{1}{1 + \mathrm{e}^{-\pi\bar{\mu}}} \left(2 \int_{-\pi}^{0} \frac{\widetilde{G}(\vartheta)}{\widetilde{\mathcal{P}}(\vartheta)}\, \mathrm{d}\vartheta + \widetilde{G}(0)\, \mathrm{e}^{-\pi\bar{\mu}} \int_{-\pi}^{0} \frac{\mathrm{d}\vartheta}{\widetilde{\mathcal{P}}(\vartheta)} \right) - \int_{-\pi}^{0} \frac{\widetilde{G}(\vartheta)}{\widetilde{\mathcal{P}}(\vartheta)}\, \mathrm{d}\vartheta$$

$$= \frac{1}{1 + \mathrm{e}^{-\pi\bar{\mu}}} \left(\widetilde{G}(0)\, \mathrm{e}^{-\pi\bar{\mu}} \int_{-\pi}^{0} \frac{\mathrm{d}\vartheta}{\widetilde{\mathcal{P}}(\vartheta)} + (1 - \mathrm{e}^{-\pi\bar{\mu}}) \int_{-\pi}^{0} \frac{\widetilde{G}(\vartheta)}{\widetilde{\mathcal{P}}(\vartheta)}\, \mathrm{d}\vartheta \right)$$

$$= \frac{\widetilde{G}(0)\, \mathrm{e}^{-\pi\bar{\mu}}}{1 + \mathrm{e}^{-\pi\bar{\mu}}} \int_{-\pi}^{0} \frac{\mathrm{d}\vartheta}{\widetilde{\mathcal{P}}(\vartheta)} + \frac{1 - \mathrm{e}^{-\pi\bar{\mu}}}{1 + \mathrm{e}^{-\pi\bar{\mu}}} \int_{-\pi}^{0} \frac{\widetilde{G}(\vartheta)}{\widetilde{\mathcal{P}}(\vartheta)}\, \mathrm{d}\vartheta, \tag{A.8}$$

which is Eq. (6.7).

Appendix B. Notation

Table 1. Notation used in the paper, Section 2.

symbol	description
shape parameters (Section 2.1)	
$\boldsymbol{r} = (x, y)$	coordinates of point in lab (spatial) frame;
	also center of rotation of swimmer
$\boldsymbol{R} = (X, Y)$	coordinates of point in swimmer's frame;
	$(X, Y) = (0, 0)$ is center of rotation
$\boldsymbol{R}_{\mathrm{b}}(\varphi) = (X_{\mathrm{b}}(\varphi), Y_{\mathrm{b}}(\varphi))$	boundary in swimmer's frame
$\boldsymbol{r}_{\mathrm{b}}(\varphi) = (x_{\mathrm{b}}(\varphi), y_{\mathrm{b}}(\varphi))$	boundary in lab frame
θ	swimming direction w.r.t. x axis
$\mathbb{Q}_{\theta}$	rotation matrix
W	point of contact between swimmer and wall
$\boldsymbol{t}_{\mathrm{b}}$	tangent to swimmer's boundary
$y_*(\theta)$	wall distance function
X_{rot}	center of rotation offset (> 0 toward front)
ℓ	maximum swimmer diameter
a, b	ellipse semi-axis $\parallel$ and $\perp$ to swimming direction
e	ellipse eccentricity
channel geometry (Section 2.2)	
L	channel width
$\zeta_{\pm}(\theta)$	range of y in channel: $\zeta_-(\theta) \le y \le \zeta_+(\theta)$
Ω	open channel configuration space of (x, y, θ)
Ω_i	closed channel configuration space component
θ_i^{L}, θ_i^{R}	θ left and right limits of Ω_i

TABLE 2. Notation used in the paper, Sections 3 to 5.

symbol	description
stochastic model (Section 3)	
t	time
U	swimming speed
$W_i(t)$	Brownian motion
D_X, D_Y	diffusivity $\parallel$ and $\perp$ to swimming direction
D_θ	rotational diffusivity
$p(x, y, \theta, t)$	probability density of swimmers
$\boldsymbol{U} = (u, v)$	swimming velocity vector
$\mathbb{D}$, D_{xx}, D_{yy}, D_{xy}	spatial diffusivity tensor and components
$\hat{\boldsymbol{x}}$, $\hat{\boldsymbol{y}}$, $\hat{\boldsymbol{\theta}}$	unit vectors
$\boldsymbol{n}$	normal vector to boundary
$\bar{p}$, $\bar{\boldsymbol{f}}$, $\bar{\boldsymbol{n}}$	x-independent quantities for infinite channel
reduced equation (Section 4)	
$\varepsilon = D_\theta$	small expansion parameter
$\bar{p}_i$	probability density at order ε^i
$T = \varepsilon t$	dimensionless slow time
Q	solution at order ε^0 (4.4)
$\sigma = U \sin\theta / D_{yy}$	(4.4)
w	channel weight function (4.8a)
ν	channel drift for Q (4.8b)
$\mu = (\nu + w')/w$	channel drift for P (4.16)
$\Delta = \frac{1}{2}\sigma\left(\zeta_+ - \zeta_-\right)$	(4.11)
$P = wQ$	θ marginal density at order ε^0 (4.14)
invariant density (Section 5)	
$\mathcal{Q}$, $\mathcal{P}$	marginal invariant density for Q, P
$\bar{p}_0 = \mathcal{Q}\,\mathrm{e}^{\sigma y}$	invariant density
c_1, c_2	integration constants (5.3)
Φ, F	integrating factor terms (5.4)
$\mathbb{E}$	expected value over invariant marginal density $\mathcal{P}(\theta)$
$\omega = \mathbb{E}\mu = 2\pi c_2$	angular rotation rate of swimmmer
$\bar{\mu}$	θ-averaged drift (5.11)
α	diffusivity ratio D_X/D_Y
β	center-offset Péclet number $U(a - X_{\mathrm{rot}})/2D_Y$

TABLE 3. Notation used in the paper, Sections 6 and 7.

symbol	description
mean exit time (Section 6 and Appendix A)	
$\tau(\theta)$	dimensionless mean exit time to θ^{L} or θ^{R}
$\mathrm{T} = w\tau'$	(6.2)
$\widetilde{\mathcal{P}} = \tilde{c}_1\, w\, \mathrm{e}^{\Phi}$	closed-channel invariant density (6.3)
$\mathcal{C}$	integration constant
$\widetilde{G}$	(6.3)
τ_{rev}	dimensionless mean reversal time (6.7)
$\lambda = \ell/L,\ \delta = 1 - \lambda$	narrow exit parameters (6.11)
$\tilde{\Phi}$	periodic part of Φ (A.3)
homogenized equation (Section 7.1)	
η	scale separation parameter (7.2a)
p_i	probability density at order η^i
$\mathcal{L}$	linear operator (7.2a)
$\langle \cdot \rangle$	cell integral (7.4)
P	large-scale probability density (7.12)
ρ	cell-normalized invariant density (7.6)
χ	solution to cell problem (7.9)
D_{eff}	effective diffusivity (7.13)
D_{enh}	enhanced diffusivity (7.24)
reduced equation (Sections 7.2 and 7.3)	
χ_i	χ at order ε^i (7.14)
X	solution at order ε^0 (7.15)
Ξ	right-hand side of X equation (7.17)
H	(7.19)
d_i	integration constants